

---


Electronic Theses and Dissertations, 2004-2019

---

2015

## Synthesis and Characterization of Core-Shell Zinc Silica Nanoparticles and Zinc Silica Nanogels for Agricultural Applications.

Megan Berroth  
*University of Central Florida*

 Part of the [Biotechnology Commons](#), and the [Molecular Biology Commons](#)  
Find similar works at: <https://stars.library.ucf.edu/etd>  
University of Central Florida Libraries <http://library.ucf.edu>

This Masters Thesis (Open Access) is brought to you for free and open access by STARS. It has been accepted for inclusion in Electronic Theses and Dissertations, 2004-2019 by an authorized administrator of STARS. For more information, please contact [STARS@ucf.edu](mailto:STARS@ucf.edu).

---

### STARS Citation

Berroth, Megan, "Synthesis and Characterization of Core-Shell Zinc Silica Nanoparticles and Zinc Silica Nanogels for Agricultural Applications." (2015). *Electronic Theses and Dissertations, 2004-2019*. 5028. <https://stars.library.ucf.edu/etd/5028>

SYNTHESIS AND CHARACTERIZATION OF CORE-SHELL ZINC SILICA NANOPARTICLES  
AND ZINC SILICA NANOGELS FOR AGRICULTURAL APPLICATIONS

by

MEGAN BERROTH

B.S. University of Central Florida, 2012

B.S. University of Central Florida, 2012

A thesis submitted in partial fulfillment of the requirements  
for the degree of Master of Science  
in the Department of Molecular Biology and Microbiology  
in the Burnett School of Biomedical Science  
in the College of Medicine  
at the University of Central Florida  
Orlando, Florida

Summer Term  
2015

Major Professor: Swadeshmukul Santra

©2015 Megan Berroth

## ABSTRACT

Plant pathogens are a serious problem facing the agricultural industry today. Current methodologies use copper based biocides as the main form of defense. Unfortunately this can lead to damaging environmental effects and increased rates of antimicrobial resistance. In this study, antimicrobial activity of multiple alternative zinc-based nanoformulations were tested against three important plant pathogens: *Xanthomonas alfalfae*, *Pseudomonas syringae*, and *Clavobacter michiganensis*. *Xanthomonas* sub species cause Citrus canker, a devastating disease that affects millions of citrus trees worldwide while the latter two affect tomato crops. Materials synthesis was completed and the resulting nanoformulations were characterized by Atomic Absorption Spectroscopy, Scanning Electron Microscopy, High Resolution Transmission Electron Microscopy, and X-Ray Photoelectron Spectroscopy. The antimicrobial efficacy of the newly synthesized formulas and two commercially available products, Kocide 3000 (DuPont) and Nordox (Brandt), were determined by Minimum Inhibitory Concentration Assays followed by Bacterial Viability Assays. The subsequent data demonstrated a marketed difference in the way the antimicrobial agents acted upon the bacterial species. The core-shell zinc silica nanoparticles (C-SZnSiNP) proved to be ineffective, while the zinc silica nanogel (ZnSiNG) was as successful at killing the bacteria as the commercial products. This shows promise for a new alternative material with zinc at the forefront of the fight against plant pathogens.

I dedicate this work to my family - my mother Mary, brother Steven, and my wonderful husband, Jason, who helped me get to where I am today.

## ACKNOWLEDGMENT

I would like to express my gratitude first and foremost to my mentor, Dr. Santra, for his assistance and inspiration in this project, as well as furthering my education and pursuits in this field of research.

I thank my committee members Dr. Travis Jewett and Dr. Sean Moore for their service and input in my thesis.

I would like to acknowledge Dr. Helge Heinrich, Kirk Scammon and the personnel of the Materials Characterization Facility (MCF) in the Advanced Materials Processing and Analysis Center (AMPAC) at the University of Central Florida for their assistance in conducting X-Ray Photoelectron Spectroscopy, Scanning Electron Microscopy, and High-Resolution Transmission Electron Microscopy. Dr. Mathew Rex of the Chemistry Department is thanked for his assistance and training with Atomic Absorption Spectroscopy. Ernest Gemeinhart is thanked for his assistance in designing and constructing the mini-greenhouse used in the initial Phytotoxicity studies and his continuing assistance. The rest of staff of the NanoScience Technology Center are thanked for their assistance and support in my research.

I would like to especially thank Dr. Borgon and Professor Verity for their support and encouragement throughout my undergraduate and graduate career.

I sincerely thank my colleagues/friends Joshua Bazata, Mikael Young, Jeremy Tharkur, Samantha Nelson, Nickisha Pierre-Pierre, Parthiban Rajensankeran, and Tyler Maxwell for their ever-essential help.

## TABLE OF CONTENTS

LIST OF FIGURES.....	viii
LIST OF TABLES.....	xi
CHAPTER 1: INTRODUCTION.....	1
1.1 Citrus Canker and Plant Pathogens .....	1
1.2 Current Methodologies.....	2
1.3 Silica as a Vehicle .....	3
1.4 Antimicrobial Activity of Zinc.....	4
CHAPTER 2: MATERIAL SYNTHESIS .....	6
2.1 Synthesis silica nanoparticles (SiNP) .....	6
2.2 Synthesis of core-shell silica nanoparticles (C-S SiNP).....	6
2.3 Synthesis of core-shell Zn loaded silica nanoparticles (C-S ZnSiNP) .....	7
2.4 Synthesis of Zn loaded silica nanogel (ZnSiNG) .....	8
CHAPTER 3: CHARACTERIZATION .....	9
3.1 Atomic Absorption Spectroscopy.....	9
3.2 Scanning Electron Microscopy .....	9
3.3 Transmission Electron Microscopy.....	10
3.4 X-Ray Photoelectron Spectroscopy .....	10
CHAPTER 4: ANTIMICROBIAL ACTIVITY AND TOXICOLOGY .....	12
4.1 Antimicrobial Studies.....	12
4.1.1 Minimum Inhibitory Concentration (MIC).....	13
4.1.2 Alamar Blue Assay.....	13
4.1.3 Bacterial Viability.....	14

4.2 Phytotoxicity Studies.....	15
4.3 Cytotoxicity Studies .....	15
CHAPTER 5: RESULTS.....	17
5.1 Characterization.....	17
5.1.1 Atomic Absorption Spectroscopy.....	17
5.1.2 Scanning Electron Microscopy .....	17
5.1.3 Transmission Electron Microscopy.....	17
5.1.4 X-Ray Electron Spectroscopy.....	18
5.2 Antimicrobial Activity and Toxicology.....	18
5.2.1 Antimicrobial Studies.....	18
5.2.1.1 Minimum Inhibitory Concentration (MIC).....	18
5.2.1.2 Alamar Blue Assay.....	19
5.2.1.3 Bacterial Viability .....	20
5.2.2 Phytotoxicity Studies.....	20
5.2.3 Cytotoxicity Studies .....	20
CHAPTER 6: CONCLUSION .....	46
LIST OF REFERENCES .....	49



## LIST OF FIGURES

Figure 1: SEM (low magnification) image of SiNP.....	22
Figure 2: SEM image of SiNP.....	22
Figure 3: SEM image of SiNP.....	23
Figure 4: SEM (low magnification) image of C-S SiNP.....	23
Figure 5: SEM (low magnification) image of C-S SiNP.....	24
Figure 6: SEM image of C-S SiNP.....	24
Figure 7: SEM image of C-S SiNP.....	25
Figure 8: SEM (low magnification) image of C-S ZnSiNP. ....	25
Figure 9: SEM image of C-S ZnSiNP showing the rough texture of the Zn loaded outer shell. .....	26
Figure 10: SEM image of C-S ZnSiNP depicting size .....	26
Figure 11: SEM image of C-S ZnSiNP.....	27
Figure 12: SEM image of ZnSiNG.....	27
Figure 13: SEM image of ZnSiNG.....	28
Figure 14: HR-TEM (low magnification) image of SiNP.....	28
Figure 15: Field of view for selected area electron diffraction (SAED) image during HR- TEM of SiNP.....	29
Figure 16: Selected area electron diffraction (SAED) image during HR-TEM of SiNP showing amorphous nature of the silica matrix.....	29
Figure 17: Energy-dispersive X-ray spectroscopy (EDX) for elemental analysis of SiNP during HR-TEM.....	30
Figure 18: HR-TEM (low magnification) image of C-S SiNP.....	30

Figure 19: Field of view for selected area electron diffraction (SAED) image during HR-TEM of C-S SiNP.....	31
Figure 20: SAED of C-SZnSiNP .....	31
Figure 21: HR-TEM (low magnification) image of C-S ZnSiNP.....	32
Figure 22: HR-TEM (low magnification) image of C-S ZnSiNP.....	32
Figure 23: SAED of ZnSiNG.....	33
Figure 24: Energy-dispersive X-ray spectroscopy (EDX) for elemental analysis of ZnSiNG during HR-TEM.....	33
Figure 25: HR-TEM (low magnification) image of ZnSiNG.....	34
Figure 26: X-ray photoelectron spectroscopy (XPS) survey spectra of C-S ZnSiNP showing the elemental composition.....	35
Figure 27: X-ray photoelectron spectroscopy (XPS) high-resolution spectra of Zn in C-S ZnSiNP showing a majority of Zn(II) electron states.....	35
Figure 28: X-ray photoelectron spectroscopy (XPS) survey spectra of ZnSiNG showing the elemental composition.....	36
Figure 29: X-ray photoelectron spectroscopy (XPS) high-resolution spectra of Zn in ZnSiNG showing a majority of Zn(II) electron states.....	36
Figure 30: Bar graph of bacterial viability of <i>E. coli</i> by SiNP, C-SSiNP, ZnSO <sub>4</sub> , C-SZnSiNP, ZnSiNG, Kocide 3000, and Nordox at 750 ppm of metallic Zn.....	41
Figure 31: Bar graph of bacterial viability of <i>X. alfalfae</i> by SiNP, C-SSiNP, ZnSO <sub>4</sub> , C-SZnSiNP, ZnSiNG, Kocide 3000, and Nordox at 750 ppm of metallic Zn.....	41
Figure 32: Bar graph of bacterial viability of <i>P. syringae</i> by SiNP, C-SSiNP, ZnSO <sub>4</sub> , C-SZnSiNP, ZnSiNG, Kocide 3000, and Nordox at 156.25 ppm of metallic Zn. ....	42

Figure 33: Bar graph of bacterial viability of *C. michiganensis* by SiNP, C-SSiNP, ZnSO<sub>4</sub>, C-SZnSiNP, ZnSiNG, Kocide 3000, and Nordox at 625 ppm of metallic Zn ..... 42

Figure 29: Phytotoxicity testing of nanoformulations against *S. lycopersicum* (photos). ..... 44

Figure 30: Cytotoxicity data showing comparative effects of ZnSiNG to Kocide 3000 and Nordox on RAW cells. .... 45

Figure 31: Cytotoxicity data showing comparative effects of ZnSiNG to Kocide 3000 and Nordox on A549 lung carcinoma cells. .... 45

## LIST OF TABLES

Table 1: Minimum Inhibitory Concentration (MIC) of nanoformulations and controls tested against <i>X. alfalfae</i> .....	36
Table 2: Minimum Inhibitory Concentration (MIC) of nanoformulations and controls tested against <i>E. coli</i> .....	38
Table 3: Minimum Inhibitory Concentration (MIC) of nanoformulations and controls tested against <i>P. syringae</i> .....	39
Table 4: Minimum Inhibitory Concentration (MIC) of nanoformulations and controls tested against <i>C. michiganensis</i> .....	40
Table 5: Phytotoxicity rating of nanoformulations against <i>S. lycopersicum</i> .....	43

## CHAPTER 1: INTRODUCTION

### 1.1 Citrus Canker and Plant Pathogens

Citrus canker is a disease that affects the majority of citrus species in the world. Its eradication from the industry is very important and that can be seen in the amount of money spent by citrus growers and the work conducted by researchers. The disease is a result of an infection of the plant tissue by *Xanthomonas citri* *pv. citri*, a gram-negative rod shaped bacteria. All of the above ground tissues are susceptible to bacterial infection in the last half of the expansion growth phase, and the pathogen enters through the stomates and wounds. Within less than a week, under optimal conditions, cells can begin to emerge from the leaves and serves as an inoculum for further infection (Graham, Gottwald et al. 2004). Lesions on the fruit, leaves, and branches of the citrus tree characterize the resulting effects of the infection. The blemished fruit cannot be sold and some of the fruit will drop prematurely, producing a bitter juice, which cannot be used. All of this adds to loss of revenue and product for the growers. Due to the ability of *Xanthomonas citri* *pv. citri* to spread from population to population and the global trade industry, foreign countries place quarantines on exposed fruit which is costly due to increased fees (Graham, Gottwald et al. 2004). This bacterium is slow growing, and does not live long outside of the plant. Its viability is low on exposure to sunlight and it does not survive well in soil (Graham, Gottwald et al. 2004). This makes it a good candidate for eradication, which has been done before. During the early 2000s, outbreaks were controlled in Florida by removing any potentially exposed trees and destroying them.

In a list of the top ten bacterial pathogens, *Xanthomonas* species take up spots 4, 5, and 6 (*citri*) with *Pseudomonas syringae* leading the pack at 1, and *Clavibacter*

*michiganensis* (*michiganensis*) narrowly missing out (Mansfield, Genin et al. 2012). *Pseudomonas syringae* infects tomatoes resulting in bacterial speck and bleeding canker in horse-chestnut. With the emergence of these diseases, there has been an increase in the economic impact of the pathogen. It also follows a similar pattern to *Xanthomonas* in how it spreads, and once a new infection has been established it also causes devastating effects (Mansfield, Genin et al. 2012). As gram negative plant pathogens, *Xanthomonas* and *Pseudomonas syringae* have similar bacteriocin production as well, indicating a potential common way of establishing a primary infection (Ghequire, Li et al. 2012). *Clavibacter michiganensis* subsp. *michiganensis* is the causal agent of bacterial wilt and canker of tomato (*Solanum lycopersicum*) and is one of the most important bacterial pathogens of tomato. Other subspecies cause disease in potato, wheat and alfalfa. *Clavibacter michiganensis* infects through wound openings or contaminated seeds, colonizing in the vasculature of the plant including the xylem vessels (Eichenlaub and Gartemann 2011). These three xylem colonizing bacteria are important part of research concerning plant resistance to genes and the development of resistant cultivars (Bae, Han et al. 2015)

## 1.2 Current Methodologies

Currently on the market copper-based antimicrobial agents dominate. Commercially available products include Magna-Bon (copper sulfate) and Kocide 3000 (DuPont) ,a copper hydroxide based material.

Copper build up can have a potentially hazardous effect on the environment by causing oxidative stress to plants and non-target organisms. Copper toxicity has significant effects on root growth and begins before effects are seen above ground. It results in

necrosis and a predisposition to fungal attacks. Molecularly, excess copper can reduce iron uptake, furthering the damaging effects on the plants(Reichman 2002). Frequent copper applications may result in adverse effects on the environment with toxic ionic copper binding to organic matter in the soil. Copper leaching and toxicity is increased by the drop in soil pH greatly effecting trees in the area (Behlau, Belasque Jr et al. 2010). Large amounts of copper based biocides have been used in the agricultural industry resulting in an increased prevalence of copper-resistant strains of bacterial plant pathogens and to a reduction of disease control (Behlau, Canteros et al. 2011). In *P. syringae* the copper resistance mechanism is conferred by the operon *copABCD*, which has similarities to the plasmid-borne genes for copper resistance in *Xanthomonas* subspecies. Nurseries then become hot spots for these strains and infections to spread to new trees.

It is clear that copper will need to be phased out of use, and in some cases use of these products had been terminated. Zinc provides an excellent alternative metal to this problem. No zinc only product is currently available commercially to the best of our knowledge, and is therefore the subject of our investigation.

### 1.3 Silica as a Vehicle

Silica possesses excellent surface chemistry, it is chemically and thermally stable, has high biocompatibility, and is relatively transparent. This makes it an excellent candidate for use in applied nanotechnology. The use of nanoparticles increases the surface area of the antimicrobial agent that in turn could increase the amount of contact with the bacterial cells. Nanoparticles can overcome existing drug resistance mechanisms, including biofilm formation and intracellular bacteria as well as provide a targeted approach to

antimicrobial agent delivery to the infection site (Pelgrift and Friedman 2013). This technology can be applied to a variety of situations, including agricultural applications. Because of these properties, a core-shell zinc loaded silica nanoparticle (C-S ZnSiNP) was developed. The term “core-shell” refers to the synthesis and structure of the final C-S ZnSiNP. The Stober process is a method of synthesizing uniform, colloidal spheres from a silica alkoxide in the presence of an alcohol and ammonia at room temperature. This causes the condensation and hydrolysis of the silica alkoxides, forming the finished particle. In the case of a core-shell silica nanoparticle, the Stober process is used to form a “seed” particle. A zinc silica nanogel is then synthesized around the “seed” by using an acid based, modified Stober method with zinc sulfate heptahydrate as the zinc donor. The use of a core shell system allows the zinc to be added only to the surrounding surface, minimizing waste of materials and increasing the availability of the zinc itself.

#### 1.4 Antimicrobial Activity of Zinc

Zinc is the fourth most widely used metal in the world after iron, aluminum, and copper. It has been used for thousands of years in various industries since at least 2000 B.C. (Moezzi, McDonagh et al. 2012). Zinc is a known micronutrient and at non-toxic levels, zinc is essential to the growth of microbes. It functions as a main component or activator of many important enzymes, and maintains the integrity of ribosomes, membranes, and dsDNA (Babich and Stotzky 1978). A tolerance to zinc could be related to this requirement or variations in absorption of this essential ion.

The mechanism of this negative interaction has been largely unknown. Researchers have suggested that excess  $Zn^{2+}$  may interfere with  $Mg^{2+}$  (Babich and Stotzky 1978).



Despite this fact, the toxicity of zinc on bacteria and fungi has long been demonstrated. In our group's previous studies with multiple metallic nanoformulations, a dose dependent factor has been demonstrated in killing the bacteria as well. A mechanism was proposed in 2011 in *Streptococcus pneumoniae*, which stated that  $Zn^{2+}$  was able to bind to a solute binding protein PsaA (McDevitt, Ogunniyi et al. 2011). PsaA normally binds  $Mn^{2+}$  and transports it into the cell, but  $Zn^{2+}$  has the ability to bind in a weaker but more temperature stable way than  $Mn^{2+}$  does to the protein. This causes the microorganism to be starved of the nutrient  $Mn^{2+}$  which plays an important role in its survival and virulence (McDevitt, Ogunniyi et al. 2011). In a study with ZnO NP, it was hypothesized that the release of damaging  $Zn^{2+}$  to the cell membrane in conjunction with lethal hydroxyl radicals that formed as a part of the interactions of ZnO NP and water lead to the antimicrobial activity of zinc against *Escherichia coli* and *Candida albicans* (Hsueh, Ke et al. 2015)

## CHAPTER 2: MATERIAL SYNTHESIS

### 2.1 Synthesis silica nanoparticles (SiNP)

This follows the steps used to create the core silica particle. 1.3 mL of tetraethyl orthosilicate (TEOS) was combined with 5.7 mL of ethanol (EtOH) (95% V/V) in a glass vial. In a flask with a magnetic stir bar, 13 mL ethanol (95% V/V), 7 mL ammonium hydroxide (30% V/V), and 3 mL deionized water (dH<sub>2</sub>O) were added. The TEOS/EtOH mixture was then added while still stirring and the mixture was allowed to synthesize for 1 hour at 400 rpm. After synthesis, this mixture was sonicated in a water bath for 10 minutes, followed by centrifugation at 10,000 rpm for 10 minutes. Then they were washed, the pH checked with a Mettler Toledo pH meter, and stored in deionized water. (Rossi, Shi et al. 2005)

### 2.2 Synthesis of core-shell silica nanoparticles (C-S SiNP)

The synthesis of C-S SiNP follows the previous procedure and adds a silica “shell” to the outside of the core particles. After the above procedure is completed (minus washing steps), the core particles were resuspended in ethanol (95% V/V). In preparation for step two; 75 µL of 1% hydrochloric acid, 25 mL dH<sub>2</sub>O, and 650 µL TEOS were combined. The acidulated TEOS mixture was combined with the seed particles while magnetically stirring. This acid catalyzed reaction was allowed to proceed for 24 hours. After 24 hours, the C-S SiNP were sonicated for 10 minutes in a water bath, followed by centrifugation at 10,000 rpm for 10 minutes and washed with ethanol (95% V/V). The pH was checked with a

Mettler Toledo pH meter, and the final product stored in dH<sub>2</sub>O. (Maniprasad and Santra 2012)

### 2.3 Synthesis of core-shell Zn loaded silica nanoparticles (C-S ZnSiNP)

The core-shell zinc loaded silica nanoparticles were synthesized in two steps. The first procedure created the silica only core nanoparticle or “seed nanoparticle” via a base hydrolysis method that will later be charged with zinc in step two. To create the core silica particle, 1.3 mL of tetraethyl orthosilicate (TEOS) was combined with 5.7 mL of ethanol (95% V/V) in a glass vial. In a flask with a magnetic stir bar, 13 mL ethanol (95% V/V), 7 mL ammonium hydroxide (30% V/V), and 3 mL deionized water (dH<sub>2</sub>O) were added. The TEOS/ethanol mixture was then added while still stirring and the mixture was allowed to synthesize for 1 hour at 400 rpm. After synthesis, this mixture was sonicated in a water bath for 10 minutes, followed by centrifugation at 10,000 rpm for 10 minutes. The core particles were resuspended in ethanol (95% V/V). In preparation for step two; 75 μL of 1% hydrochloric acid, 25 mL dH<sub>2</sub>O, and 650 μL TEOS were combined with zinc sulfate (ZnSO<sub>4</sub>•7H<sub>2</sub>O, MW: 287.54). The TEOS/1%HCl/ZnSO<sub>4</sub> mixture was combined with the seed particles while magnetically stirring. This acid catalyzed reaction was allowed to proceed for 24 hours. After 24 hours, the C-S ZnSiNP were sonicated for 10 minutes in a water bath, followed by centrifugation at 10,000 rpm for 10 minutes and washed with ethanol (95% V/V). The pH was checked a Mettler Toledo pH meter, adjusted to 7, and the final product stored in dH<sub>2</sub>O. (Maniprasad and Santra 2012)

#### 2.4 Synthesis of Zn loaded silica nanogel (ZnSiNG)

A zinc silica nanogel was synthesized following an acid hydrolysis protocol. In a beaker, 110 mL of deionized water was acidified using 330  $\mu\text{L}$  of 1% hydrochloric acid solution (made from concentrated hydrochloric acid). 5 g of zinc sulfate ( $\text{ZnSO}_4 \cdot 7\text{H}_2\text{O}$ , MW: 287.54) was then added and stirred until dissolved. At this point 778  $\mu\text{L}$  of tetraethylorthosilicate (TEOS) was added drop-wise using a micropipette (Eppendorf) and left to stir for 24 hours. The pH of the solution was measured using a Mettler Toledo pH meter and adjusted to 7. (Young and Santra 2014)

## **CHAPTER 3: CHARACTERIZATION**

### **3.1 Atomic Absorption Spectroscopy**

Atomic absorption spectroscopy (AAS) is a technique used to measure trace metals. In this application, AAS was used to confirm zinc loading into the nanoformulations, and determine how much metallic zinc was leftover after washing steps were completed. A Perkin Elmer Analyst 400 AA flame spectrometer and a Cary Win UV-Vis Spectrometer was used to complete the assay.

Samples were prepared by first lyophilizing (LabConco FreeZone 4.5 Liter Freeze Dry System Model 7750020). The 10 g of the dry powdered material was then combined with 25 ml concentrated nitric acid under magnetic stirring conditions and heat within a fume hood. Then sample was diluted with deionized water to 100 ml total volume. The samples were then compared against zinc standards (1% nitric acid) at concentrations of 0.2, 0.5, 1, 2, 3, 5, 10, 15, 20, 25 ppm metallic zinc(L. Kotz 1972, Bader 2011).

In a separate preparation, 10 ml of each nanomaterial were lyophilized. The zinc was then extracted using a saturated ethylenediaminetetraacetic acid (EDTA) solution. These were again compared against zinc standards.

### **3.2 Scanning Electron Microscopy**

Scanning electron microscopy (SEM) was used to determine overall morphology and size of the materials developed.

Samples were prepared by spin coating silica wafers with material. Each wafer was then gold coated using a gold sputter coater (EMITECH) at UCF-AMPAC-MCF before being

loaded onto a stage and inserted into the Zeiss ULTRA-55 FEG SEM. Analysis was completed with the assistance of Mikaeel Young.

### 3.3 Transmission Electron Microscopy

In preparation for Transmission Electron Microscopy, aliquots of each material were prepared and sonicated overnight. Carbon filmed gold (Au) grids (400 square mesh, Electron Microscope Sciences) were then dipped into each nanomaterial, followed by a drop of material on each grid respectively. The grids were allowed to air dry on a Kim wipe in a petri dish. The grids were delivered to UCF-AMPAC-MCF for analysis, which was carried out by MCF personnel using a FEI Tecnai F30 TEM using a 100 KV electron beam intensity. Energy-dispersive X-ray spectroscopy, low resolution spectra, high resolution spectra, and selected area electron diffraction data were collected for each nanoformulation and analyzed using Digital Micrograph software.

### 3.4 X-Ray Photoelectron Spectroscopy

X-Ray photoelectron spectroscopy (XPS) is a technique used to measure the oxidation states of elements (not H or He) found in the top 10 nm of the surface of a material.

Samples were lyophilized and delivered to a UCF-AMPAC-MCF technician who loaded them onto the Physical Electronics 5400 ESCA (XPS). A survey scan (broad elemental spectrum) and a high-resolution spectra (specific for oxygen, carbon, and zinc) were collected for all nanoformulations. Zinc valence information was analyzed by

AugerScan software. The National Institute of Standards and Technology (NIST) XPS database was used to determine zinc valence states.

## CHAPTER 4: ANTIMICROBIAL ACTIVITY AND TOXICOLOGY

### 4.1 Antimicrobial Studies

To determine the antimicrobial activity of the zinc based nanoformulations a selection of experiments were performed including Minimum Inhibitory Concentration (MIC), Alamar Blue Assay, and Colony Forming Units count. C-S ZnSiNP and ZnSiNG were tested against gram-negative *Xanthomonas alfalfae* subsp. *citrumelonis* (*X. alfalfae*, ATCC 49120), gram-negative *Escherichia coli* (*E. coli*, ATCC 35218), gram-negative *Pseudomonas syringae* pv *syringae* (*P. syringae*, ATCC 19310), and gram-positive *Clavibacter michiganensis* subsp. *michiganensis* (*C. michiganensis*, ATCC 10202) organisms. All bacteria were obtained from American Type Culture Collection (ATCC) and UCF Department of Molecular Biology and Microbiology Preparatory Laboratory, University of Central Florida, Orlando, FL. *E.coli* was sub-cultured and maintained using LB agar and broth and all growth and experiments conducted at 37°C. *X. alfalfae* was subcultured and maintained using NB agar and broth with all growth and experiments conducted at 28°C. *P. syringae* was subcultured and maintained using NB agar and broth with all growth and experiments conducted at 26°C. *C. michiganensis* was subcultured and maintained using BHI agar and broth with all growth and experiments conducted at 26°C. Bacterial concentrations of 0.5 McFarland Standard (10<sup>8</sup> CFU/mL) were used. C-S ZnSiNP and ZnSiNG were compared to Nordox, Kocide® 3000, and Zinc Sulfate as positive controls with SiNP and C-S SiNP as negative controls.



#### 4.1.1 Minimum Inhibitory Concentration (MIC)

The Minimum Inhibitory Concentration (MIC) of C-S ZnSiNP and ZnSiNG were determined along with Nordox, Kocide® 3000, Zinc Sulfate with equivalent Cu concentrations along with and SiNP and C-S SiNP. MIC testing was carried out using broth microdilution in accordance with the guidelines of the Clinical and Laboratory Standards Institute (CLSI). The accuracy of the MIC determination was improved by adding 5  $\mu\text{L}$  of Alamar blue dye per 100  $\mu\text{L}$  well volume and observing color changes (blue to pink for live organisms). This reduced an error produced from the cloudiness of the nanomaterial and control materials with broth (Young and Santra 2014)

#### 4.1.2 Alamar Blue Assay

The bacterial growth inhibition studies for the C-S ZnSiNP and ZnSiNG with controls were conducted using an Alamar blue assay with a microplate reader. Briefly, different volumes of C-S ZnSiNP and controls (5, 10, 15, 20, and 25  $\mu\text{L}$ ) were prepared in sterile MH2 or LB broth in separate wells within a 96-well flat-bottom, polystyrene microplate. Uniform growth potential was ensured by each well containing an equal amount of broth and equal final volumes (200  $\mu\text{L}$ ). Each well contained  $\sim 10^5$  CFU/mL of bacteria. Appropriate “blank” wells were prepared containing no bacteria to compare with samples to determine bacterial growth. Microplates were incubated at the appropriate temperature for each bacterial species on a shaker at 200 rpm for 20–24 h. After incubation, 10  $\mu\text{L}$ /well of Alamar blue dye was added to each well followed by further incubation. After 60 min of incubation, the absorbances of each well at both 570 and 600 nm were measured. Wells containing sterile media with material controls and Alamar blue served as negative

controls. Alamar blue assays for each bacterial strain were conducted at least three times to verify the results for reproducibility. The percentage reduction of the dye was calculated by using the following formula as supplied by the manufacturer:

$$[(\epsilon_{ox})\lambda_2 A_{\lambda_1} - (\epsilon_{ox})\lambda_1 A_{\lambda_2}] / [(\epsilon_{ox})\lambda_1 A'_{\lambda_2} - (\epsilon_{ox})\lambda_2 A'_{\lambda_1}] \times 100$$

$\epsilon_{ox}$  is the molar extinction coefficient of Alamar blue oxidized form (blue),  $\epsilon_{red}$  is the molar extinction coefficient of Alamar blue reduced form (pink), A is the absorbance of test wells, A' is the absorbance of negative control well,  $\lambda_1 = 570$  nm, and  $\lambda_2 = 600$  nm (Young and Santra 2014)

#### 4.1.3 Bacterial Viability

The bactericidal activities of C-S ZnSiNP and ZnSING with controls were determined by colonyforming unit (CFU) assay. The zinc concentration (750  $\mu\text{g}/\text{mL}$ ) that produced a significant decrease in viability over the lower concentration (150  $\mu\text{g}/\text{mL}$ ) as observed in the Alamar blue assay was used to perform the CFU assay. Treatment of bacteria with nanomaterial was carried out following the same procedure as described in the Alamar blue assay. After 24 h of nanomaterial treatment with the bacteria, each sample was serially diluted in 1 $\times$  PBS and plated on LB or MH2 agar. After overnight incubation at species appropriate temperatures, individual colonies were counted.

## 4.2 Phytotoxicity Studies

Phytotoxicity studies were carried out in the plant growth and environmental chamber (Panasonic Environmental Chamber Model MLR- 352H). Specific parameters followed were simulated summer conditions (85% Relative Humidity (RH); 35 degree C). Studies were conducted using *Solanum lycopersicum*, a common tomato plant, purchased from a local Home Depot, and were used to determine their levels of tolerance to oxidative stress, depending on the material challenged, giving an idea of how toxic or useful the agricultural material can be (Young and Santra 2014)

## 4.3 Cytotoxicity Studies

To determine if there are cyto-toxic effects of nanoparticles on a murine macrophage cell line RAW264.7 The reagents CellTiter 96 Aqueous non-radioactive cell proliferation assay (Promega, Cat # G5421) or alamar blue (Invitrogen) measure the number of viable cells in the population by a calorimetric method. The Promega kit uses MTS, a tetrazolium compound that will be reduced to a formazan product by metabolically active cells. The formazan product is soluble in tissue culture medium. The absorbance of formazan at 490nm can be measured using an ELISA plate reader (Molecular devices). The quantity of formazan measured is directly proportional to the live cells. Values from untreated cells (control cells) would be considered as 100% live, and compare the values obtained with differing concentrations of PNA for % live cells. The alamar blue reagent is a resazurin based blue dye that converts into a fluorescent resorufin dye that can be detected at 590nm in a fluorescent reader. The amount of fluorescence is directly proportional to the number of viable cells. The cell viability was calculated using the following formula:

Cell viability (%) =  $OD_{490}$  of lipo-PNA/liposomes alone treated well /  $OD_{490}$  of well not treated (no liposomes) x 100

Cell viability less than 90% is considered as toxic (based on publications) and this percentage was verified by doing Trypan blue exclusion assay.

## CHAPTER 5: RESULTS

### 5.1 Characterization

#### 5.1.1 Atomic Absorption Spectroscopy

Atomic absorption spectroscopy (AAS) results indicate a loss of 50% metallic Zn concentration compared to calculated concentrations for nanoparticle. This loss takes the concentration of Zn from 10,000 ppm to 5,000 ppm.

#### 5.1.2 Scanning Electron Microscopy

SEM results confirmed the size and shape of each SiNP, C-SSiNP, and C-SZnSiNP. SiNP are uniform spherical particles of approximately 344.5 nm diameter (Figures 1, 2, 3). C-S SiNP are very similar to the SiNP with an average diameter of 362.1 nm (Figures 4, 5, 6, 7). This indicates an approximate 10 nm “shell” around the seed particle. The SEM images of C-S ZnSiNP demonstrated spherical dots of potential ZnO imbedded in the outer silica gel “shell” (Figures 8, 9, 10, 11). These particles have an average diameter of 357 nm, indicating a thinner gel layer. ZnSiNG images were taken at low resolution (Figures 12 and 13).

#### 5.1.3 Transmission Electron Microscopy

Transmission Electron Microscopy (TEM) was used to observe nanoformulations dispersion and potential crystallinity. To confirm that the microscopy was taking place using the correct location, elemental mapping was analyzed using Energy-dispersive X-ray spectroscopy (EDX), indicating the presence of Zn, Si, S, O and Au (from the TEM grid)

(Figure 17). Low resolution images were taken of SiNP, C-S SiNP (Figures 14, 18). Low resolution images of C-S ZnSiNP, and ZnSiNG were taken to demonstrate the presence of electron rich material seen as dark contrast (Figures 21, 22). Selected area electron diffraction (SAED) of SiNP, C-S SiNP, C-S ZnSiNP, and ZnSiNG signified the amorphous nature of the silica matrix and crystallinity of Zn materials (Figures 15, 16, 19, 20).

#### 5.1.4 X-Ray Electron Spectroscopy

Zinc valence states were analyzed using X-ray photoelectron spectroscopy (XPS). A Survey spectra was collected for SiNP, C-S SiNP, C-S ZnSiNP, and ZnSiNG to confirm elemental mapping showing the presence of Zn, Si, S, O, and C (Figure 23). High resolution spectra of Zn within C-S ZnSiNP and ZnSiNG was carried out to identify the Zn compounds with the nanomaterials (Figure 24). Curve fitting and referencing through the National Institute for Science and Technology (NIST) XPS database indicated the Zn compounds were ZnSO<sub>4</sub>, Zn(OH)<sub>2</sub>, ZnO, and metallic Zn. This confirmed that the most common state of zinc was in Zinc (II) compounds.

## 5.2 Antimicrobial Activity and Toxicology

### 5.2.1 Antimicrobial Studies

#### 5.2.1.1 Minimum Inhibitory Concentration (MIC)

MIC results indicate mixed results for zinc based silica nanoformulations. C-S ZnSiNP showed very minimal antimicrobial activity. However the ZnSiNG showed comparable activity to current commercial products.

In the case of *X. alfalfae*, both ZnSO<sub>4</sub> salt and ZnSiNG exhibited an MIC of 39.06ppm. This edged out both Kocide 3000 (DuPont) and Nordox (Brandt) at 156.25ppm and 78.125ppm respectively (Table 1). The same nanoformulations and controls were also run against *E. coli*. This bacteria exhibited higher resistance to the antimicrobial agents than *X. alfalfae*, which was expected and had been seen previously. Complete growth was observed for the non zinc loaded nanoparticles and C-SZnSiNP. ZnSiNG showed the greatest efficacy against *E. coli* with an MIC of 312.5 ppm along with Nordox. ZnSO<sub>4</sub> had an MIC of 625ppm and Kocide 3000 (DuPont) had a MIC of 1250ppm (Table 2). After these results were reported, further studies did not include C-SSiNP or C-SZnSiNP.

*C. michiganensis* and *P. syringae* were treated with ZnSiNG, ZnSO<sub>4</sub>, Kocide 3000, and Nordox to determine the MIC values. The ZnSiNG performed comparably to the commercial products. In *C. michiganensis*, ZnSiNG, Nordox, and Kocide 3000 came in at 78.125, 156.25, and 312.5ppm respectively (Table 3). In *P. syringae*, ZnSiNG, Nordox, and Kocide 3000 came in at 625, 625, and 312.5ppm respectively (Table 4). In both cases, the ZnSO<sub>4</sub> salt did not exhibit an MIC, resulting in full growth (Table3,4).

#### 5.2.1.2 Alamar Blue Assay

Alamar blue assays were performed on *X. alfalfae* and *E. coli*. Alamar blue dye is a colorimetric dye that is converted from an oxidized blue form to a reduced pink form by live cells. This assay gives qualitative indication of the antimicrobial effectiveness due to the color change. Taking turbidity of the materials into account, the numerical output of the equations is semiquantitative.

### 5.2.1.3 Bacterial Viability

The bacterial viability assay reported in CFU/mL was conducted to give a clear and quantitative measure of effectiveness of C-S ZnSiNP and ZnSiNG nanoformulations as well as controls. This allowed the confirmation of a bactericidal or bacteriostatic formula.

*X. alfalfae* and *E. coli* colonies were completely killed by the ZnSO<sub>4</sub> salt, with *X. alfalfae* also being completely killed by the ZnSiNG formula. Kocide 3000 (DuPont) and Nordox performed comparably across all species. These formulations were not bactericidal but did halt growth significantly and exhibited lower CFUs than the growth control. *P. syringae*, and *C. michiganensis* did not die in the presence of ZnSO<sub>4</sub>. ZnSiNG exhibited similar bacterial static activity to that of Kocide 3000 (DuPont) and Nordox.

### 5.2.2 Phytotoxicity Studies

Phytotoxicity results confirmed the hypothesis that Zn loaded nanomaterials would not cause plant tissue damage at metallic concentrations used for field trials. *Solanum lycopersicum*, the common tomato plant, did not develop lesions even after 5 days of exposure to nanoformulations. This indicates that plants have a tolerance to Zn toxicity. In comparison, the plant sprayed with the negative control, Copper Sulfate (1000 ppm), began to see damage after 2 days. Plant leaves appear to be white as the zinc based solutions dry, while the Nordox are burnt orange and the Kocide are greenish-blue. (Figure 29, Table 4).

### 5.2.3 Cytotoxicity Studies

Studies were completed by Dr. Parthiban Rajasekaran using RAW and A549 cell lines to determine the potential toxicity of the nanoformulations in question. C-S ZnSiNP



showed a similar toxicology to the controls used without the addition of Zn. This may be due to the reduction of zinc during washing steps. However, even comparing a reduction by 50% metallic zinc (example being 100 ppm of metallic zinc in C-S ZnSiNP being 50 ppm) it shows a much lower level of toxicity to the metal-based controls ( $\text{ZnSO}_4$ , Kocide 3000, Nordox). ZnSiNG has a similar toxicity to the latter (Figure 30, 31).

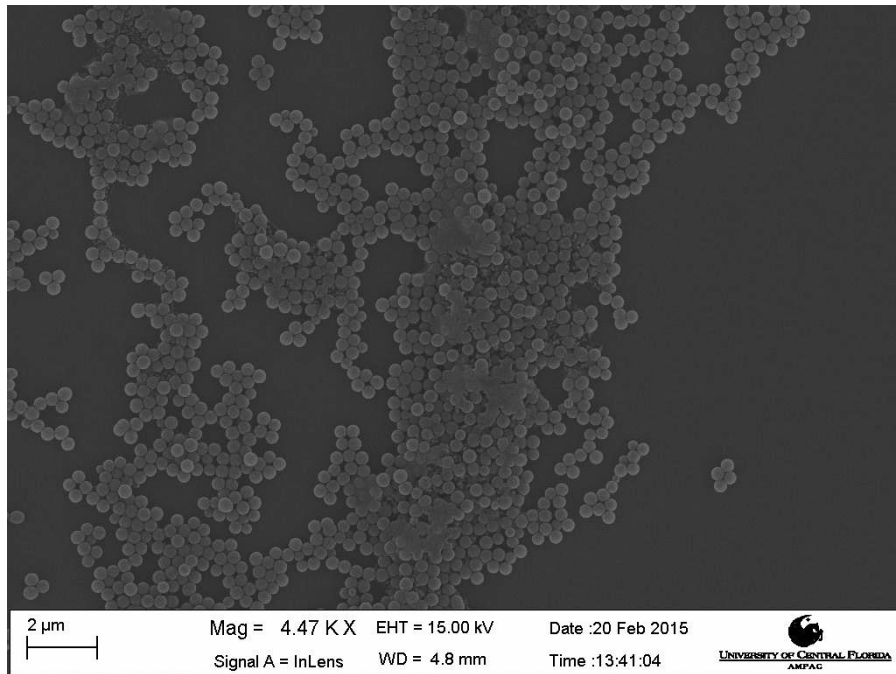


Figure 1: SEM (low magnification) image of SiNP.

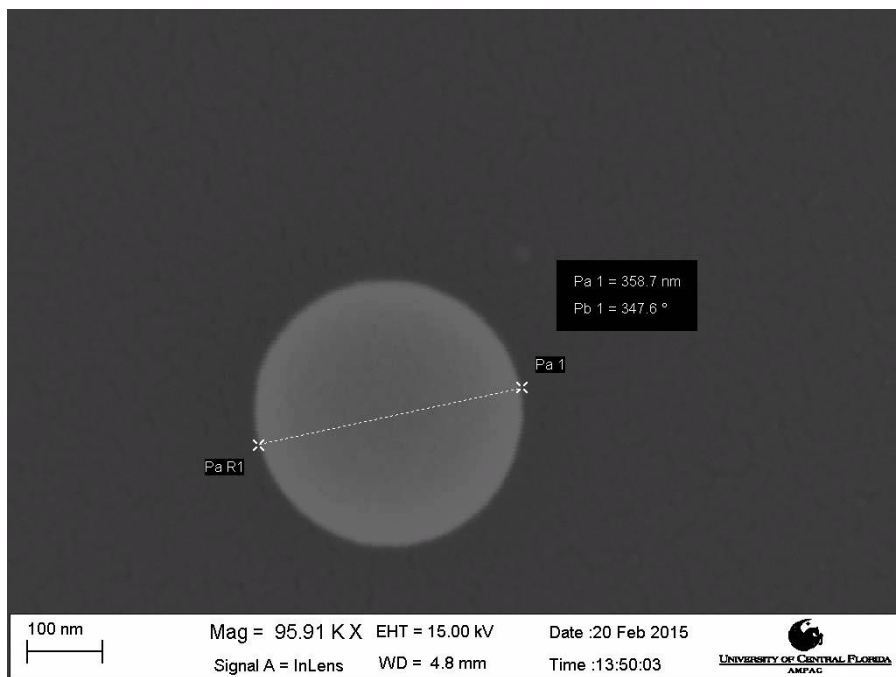


Figure 2: SEM image of SiNP.

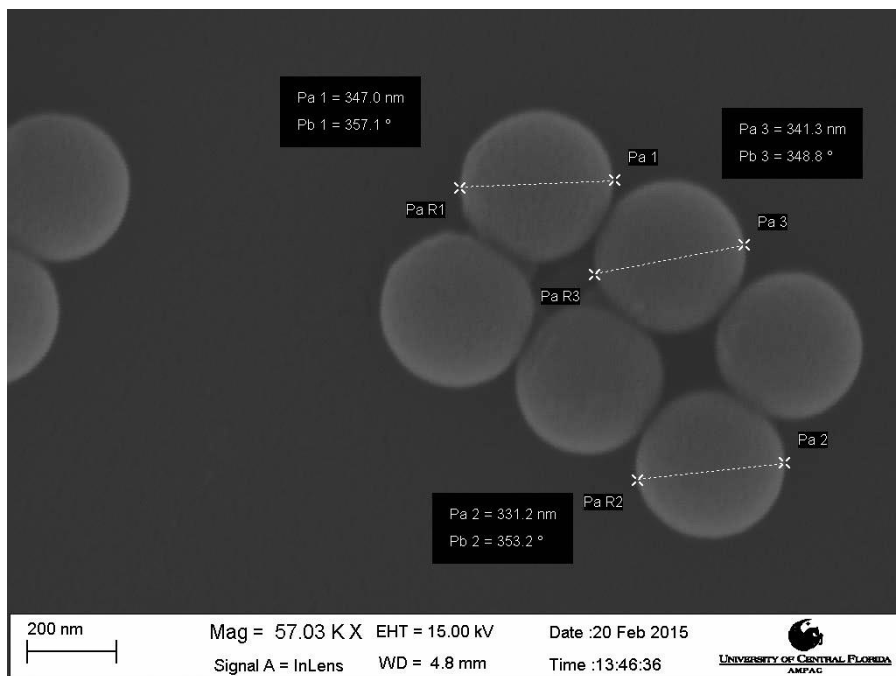


Figure 3: SEM image of SiNP.

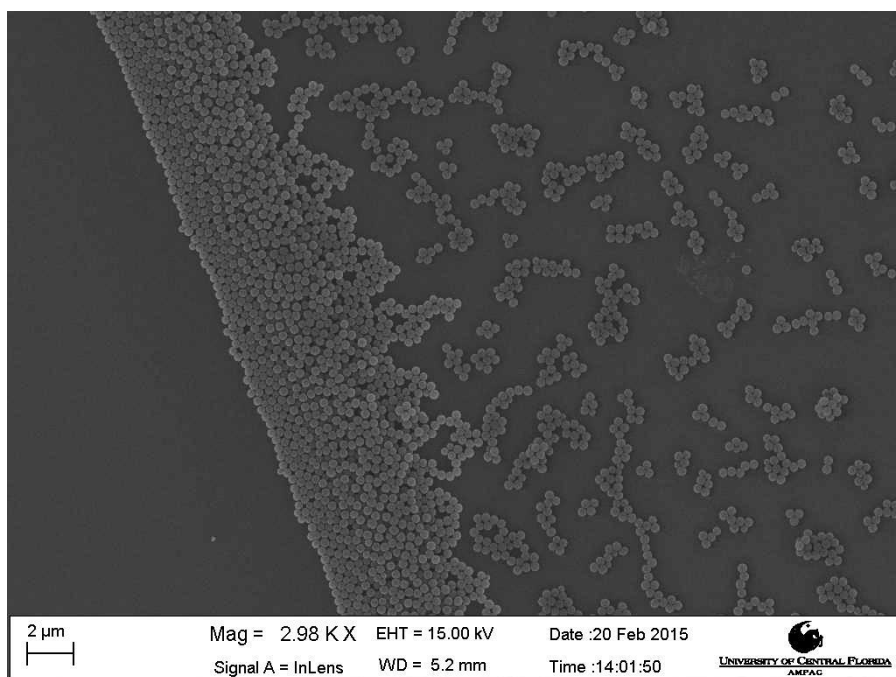


Figure 4: SEM (low magnification) image of C-S SiNP.

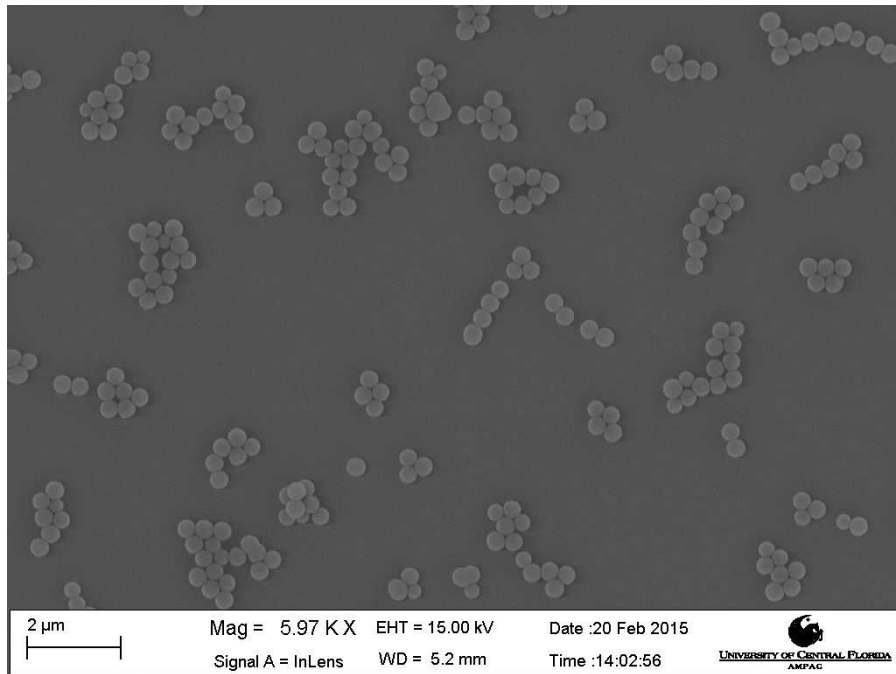


Figure 5: SEM (low magnification) image of C-S SINP.

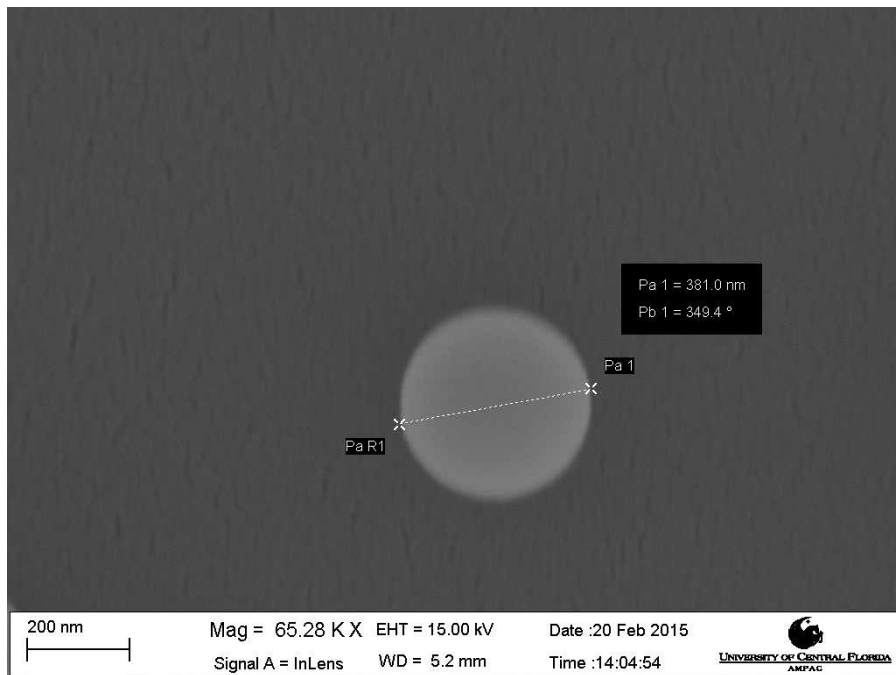


Figure 6: SEM image of C-S SINP.

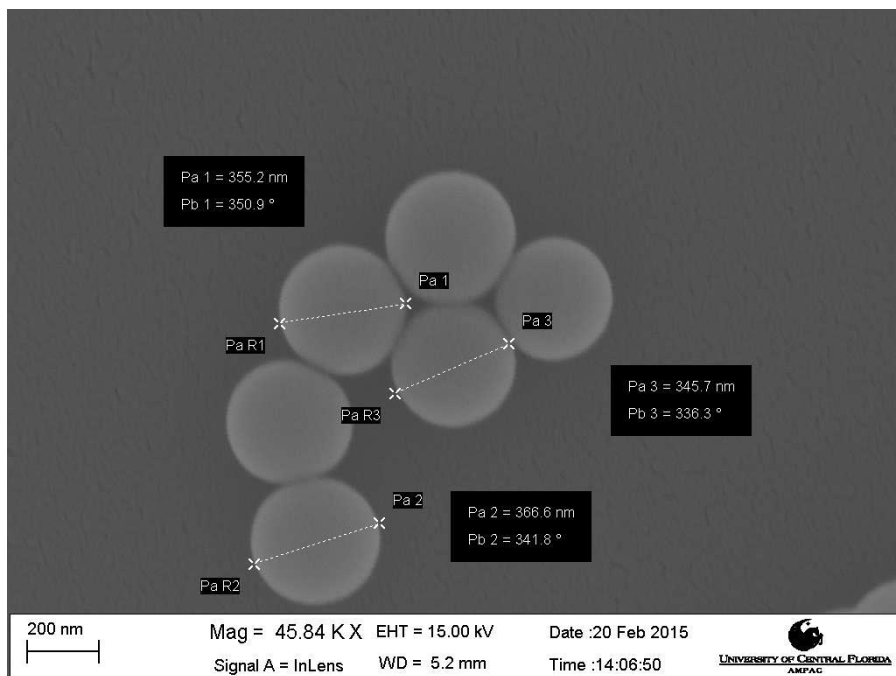


Figure 7: SEM image of C-S SINP.

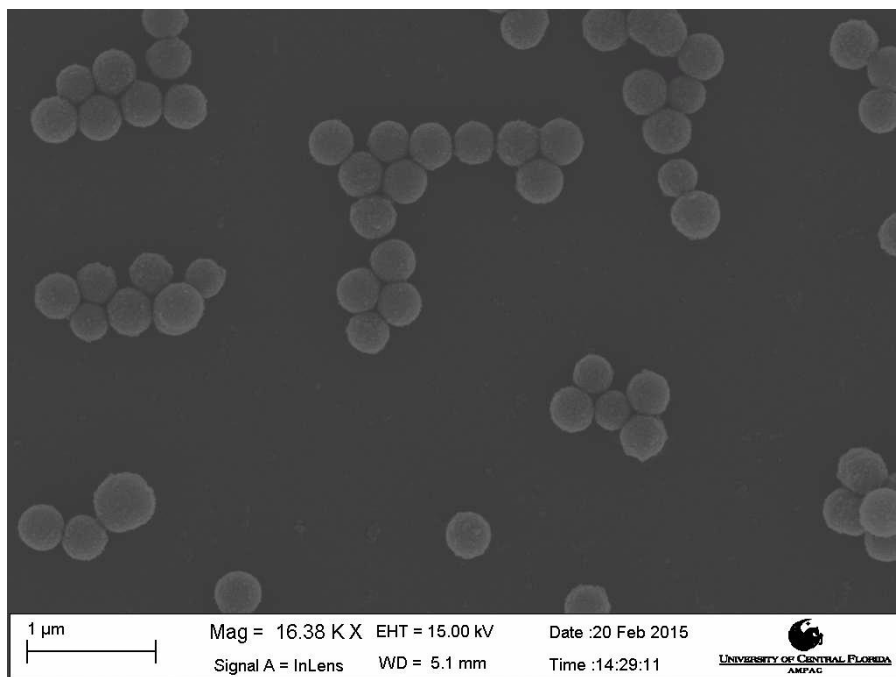


Figure 8: SEM (low magnification) image of C-S ZnSINP.

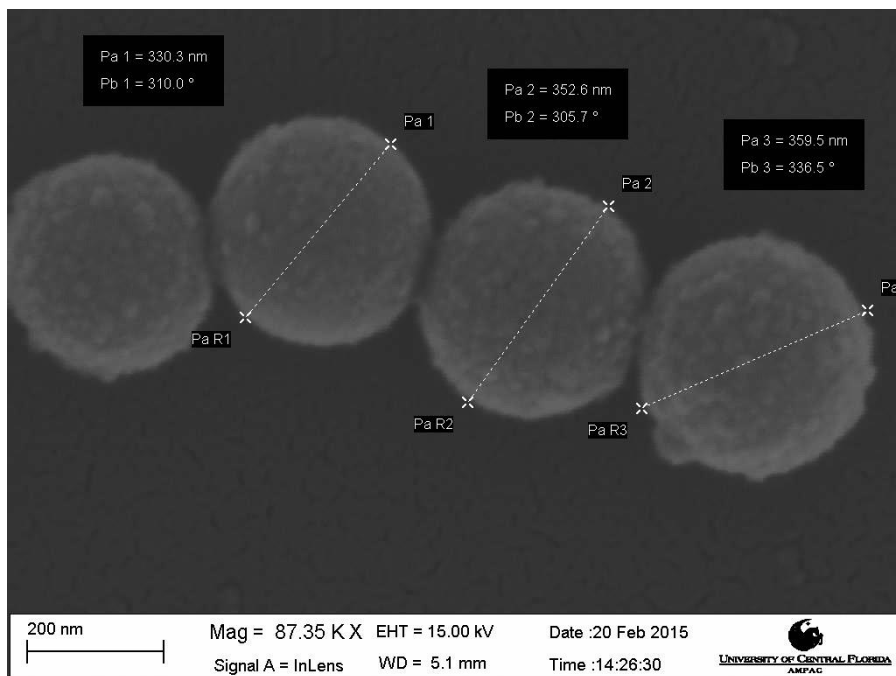


Figure 9: SEM image of C-S ZnSINP showing the rough texture of the Zn loaded outer shell.

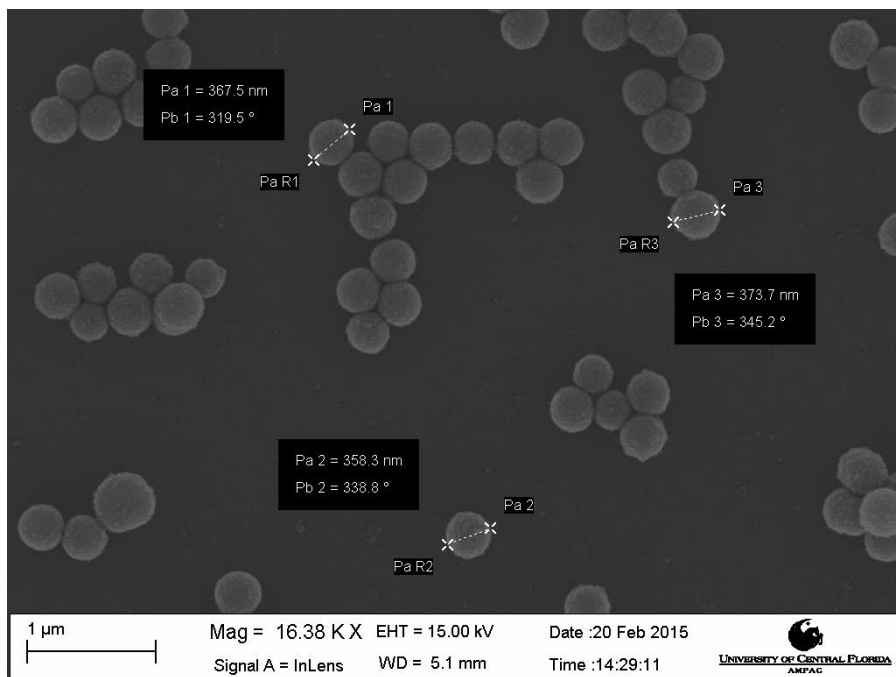


Figure 10: SEM image of C-S ZnSINP depicting size

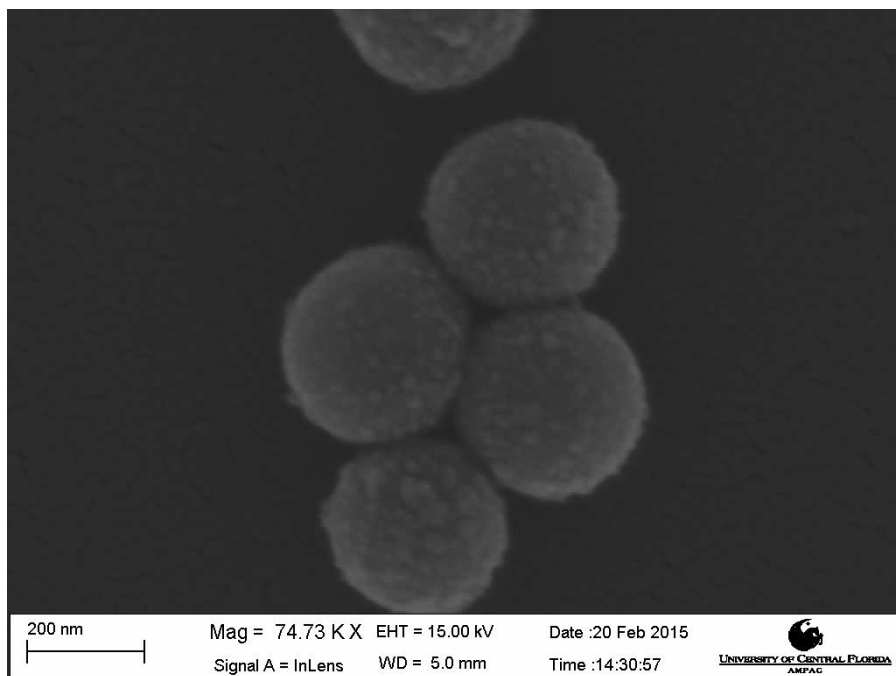


Figure 11: SEM image of C-S ZnSINP

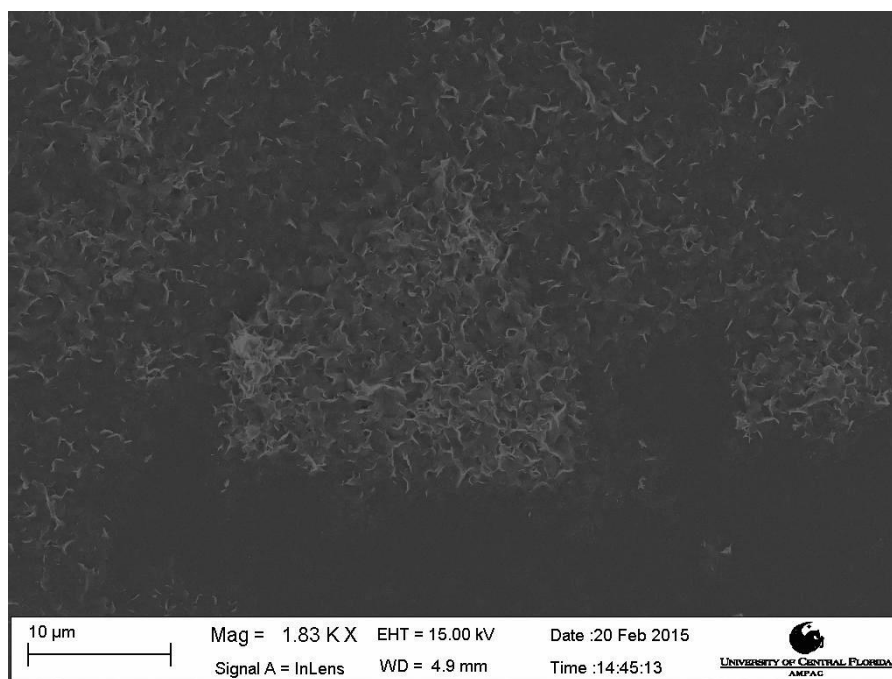


Figure 12: SEM image of ZnSiNG.

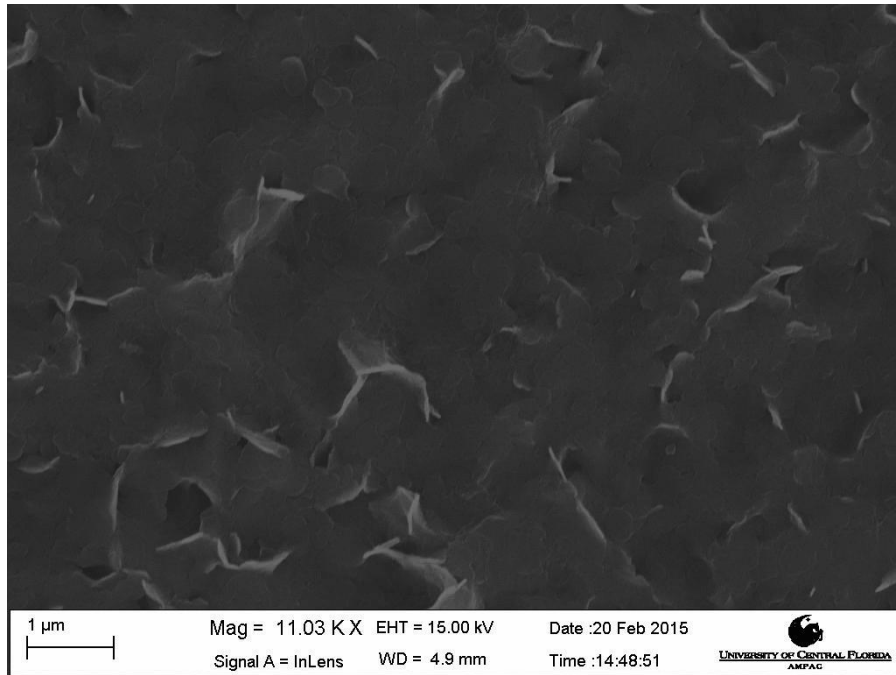


Figure 13: SEM image of ZnSiNG.

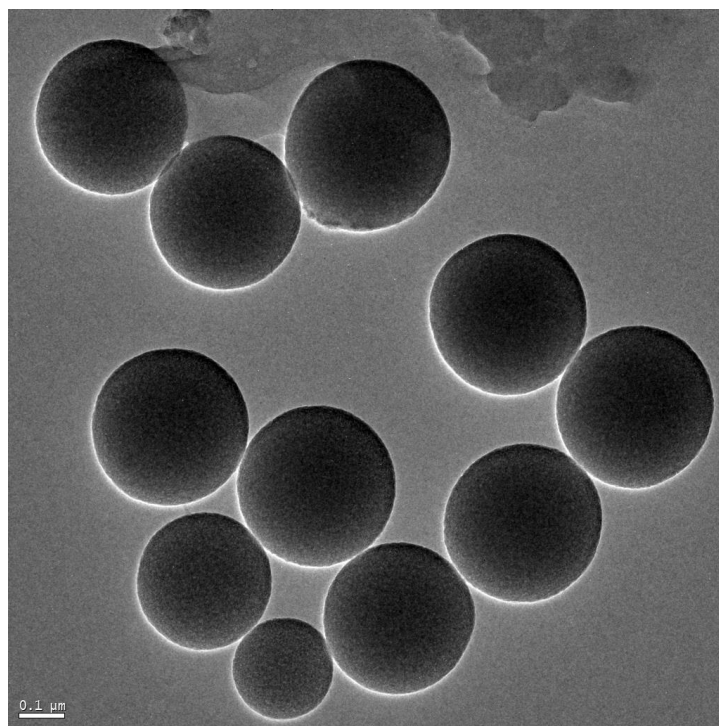


Figure 14: HR-TEM (low magnification) image of SINP.



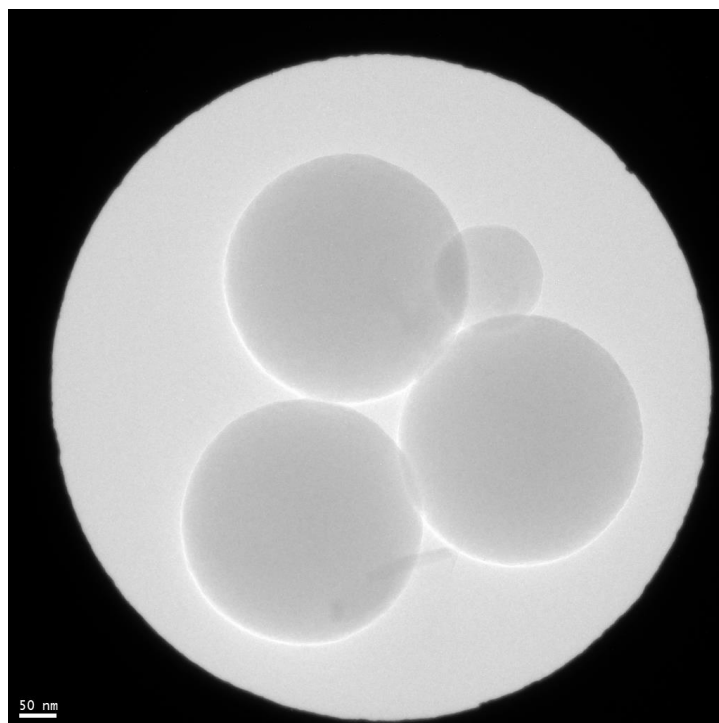


Figure 15: Field of view for selected area electron diffraction (SAED) image during HR-TEM of SINP.

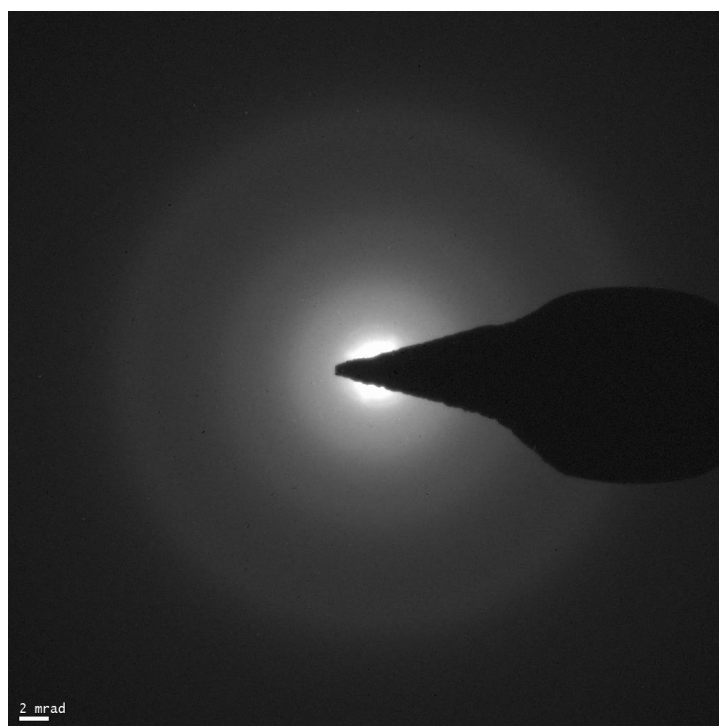


Figure 16: Selected area electron diffraction (SAED) image during HR-TEM of SINP showing amorphous nature of the silica matrix.

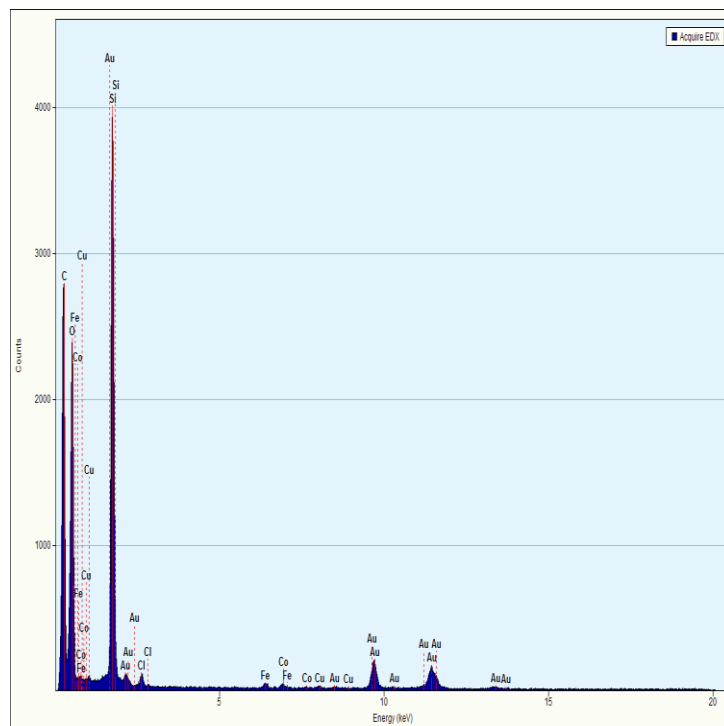


Figure 17: Energy-dispersive X-ray spectroscopy (EDX) for elemental analysis of SiNP during HR-TEM.

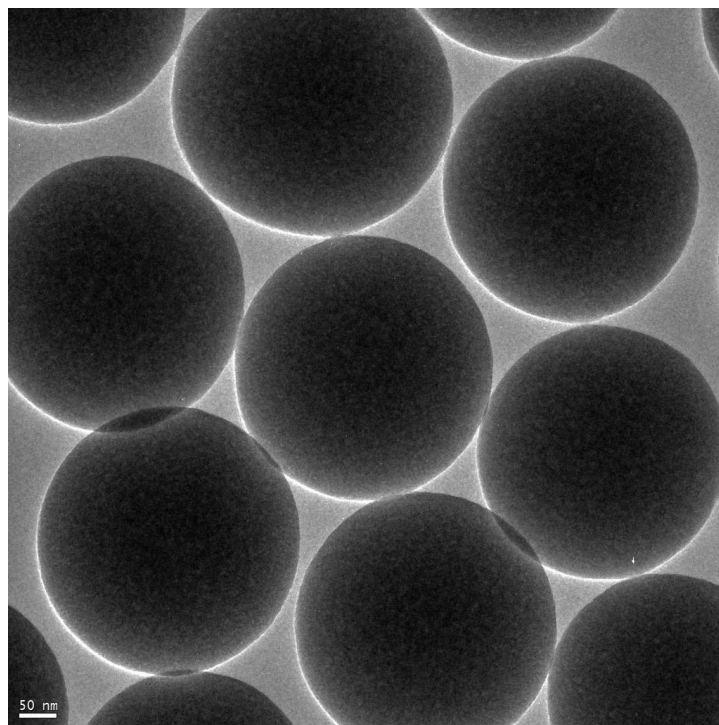


Figure 18: HR-TEM (low magnification) image of C-S SINP.

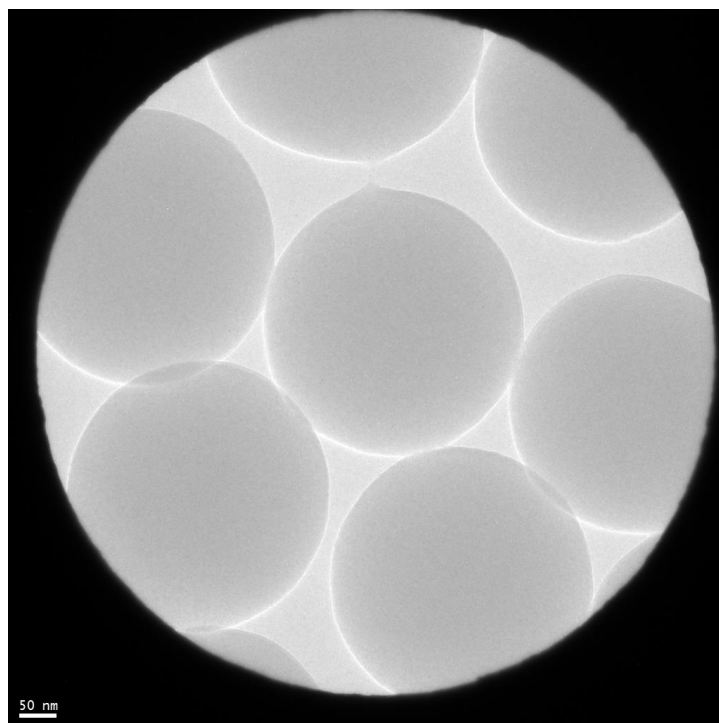


Figure 19: Field of view for selected area electron diffraction (SAED) image during HR-TEM of C-S SINP.

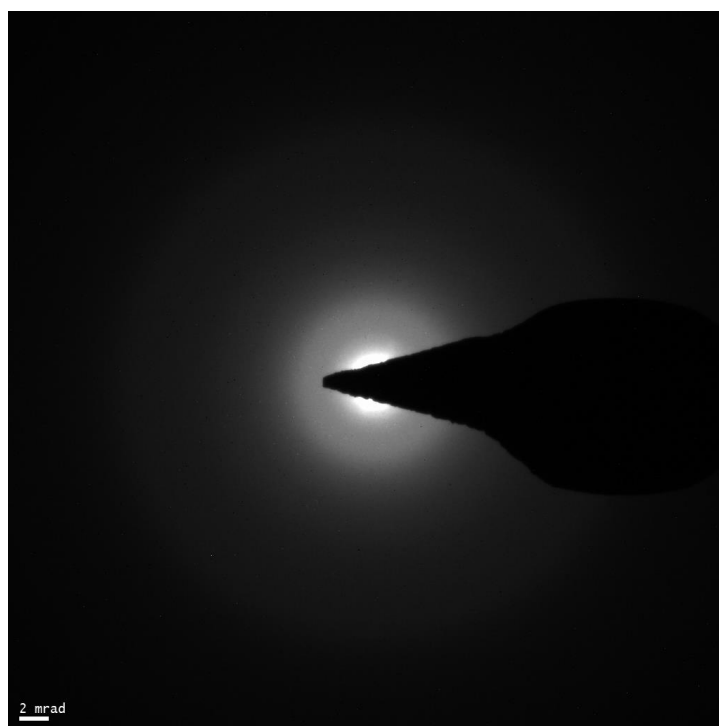


Figure 20: SAED of C-SZnSiNP

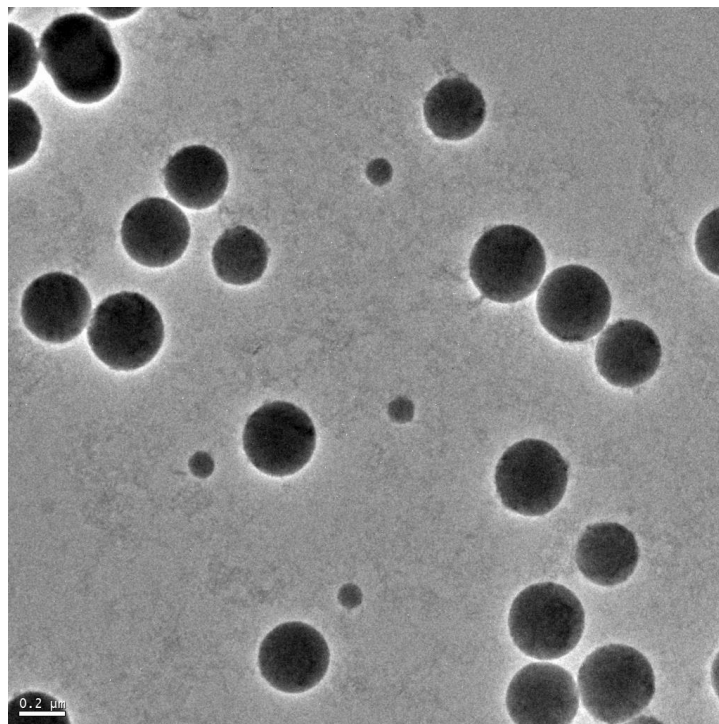


Figure 21: HR-TEM (low magnification) image of C-S ZnSINP.

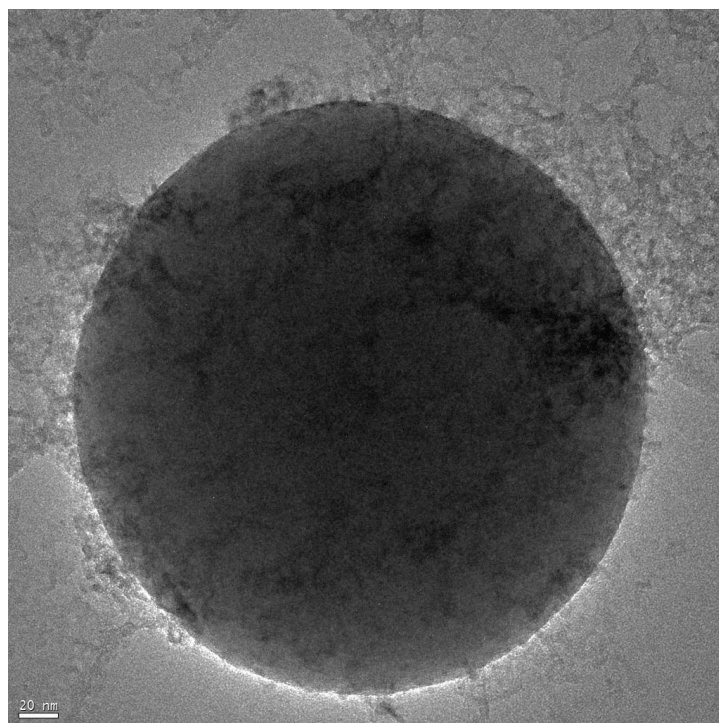


Figure 22: HR-TEM (low magnification) image of C-S ZnSINP.

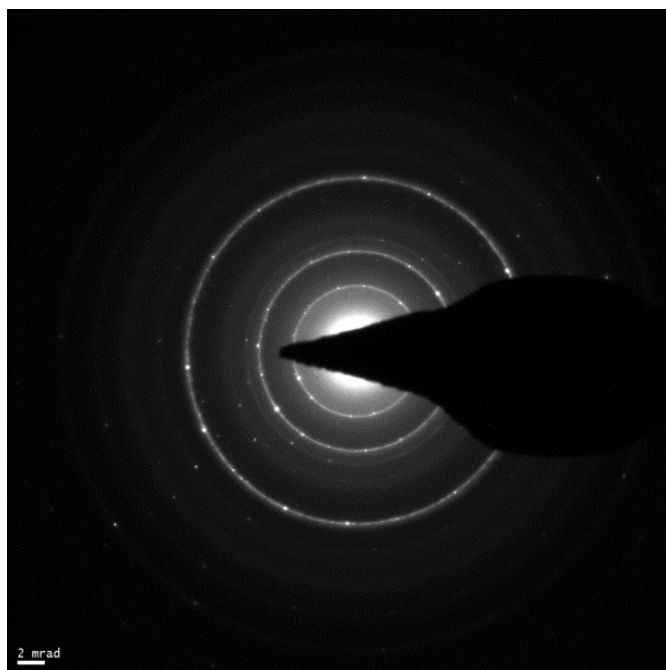


Figure 23: SAED of ZnSiNG

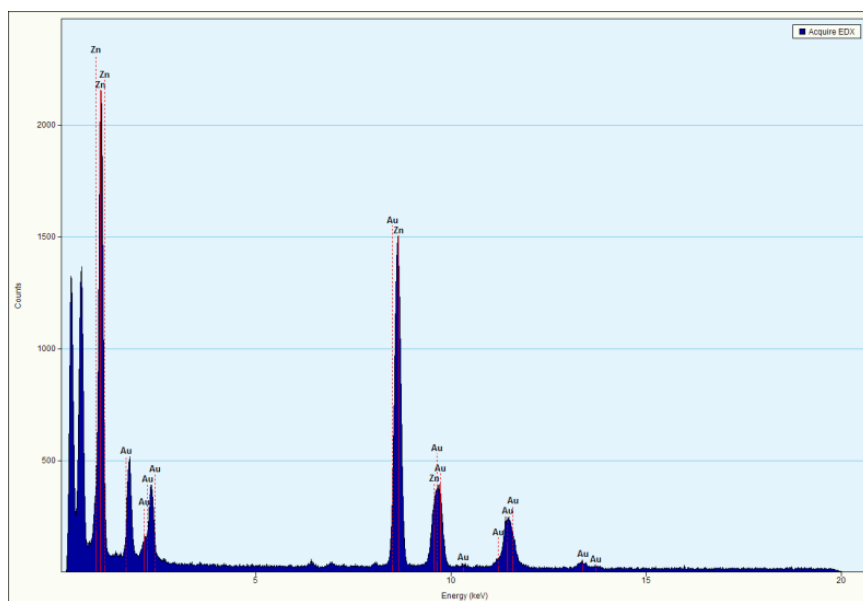


Figure 24: Energy-dispersive X-ray spectroscopy (EDX) for elemental analysis of ZnSiNG during HR-TEM.

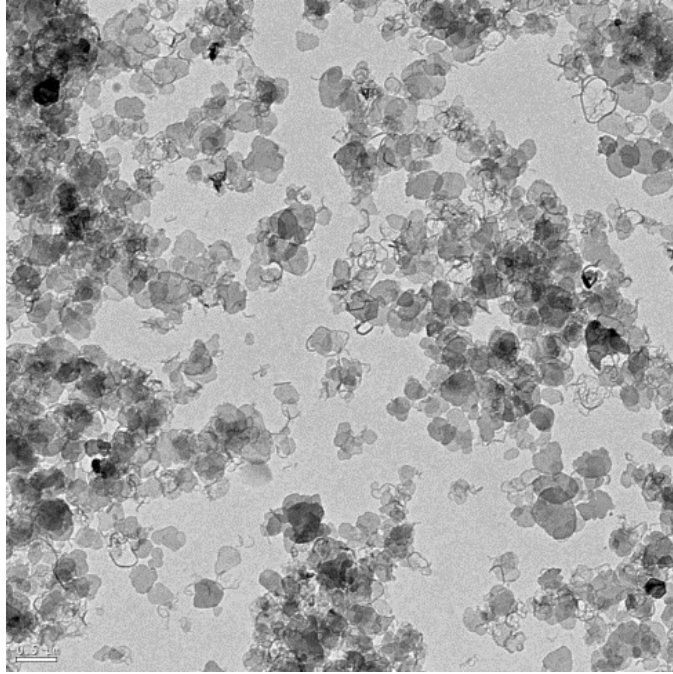


Figure 25: HR-TEM (low magnification) image of ZnSING.

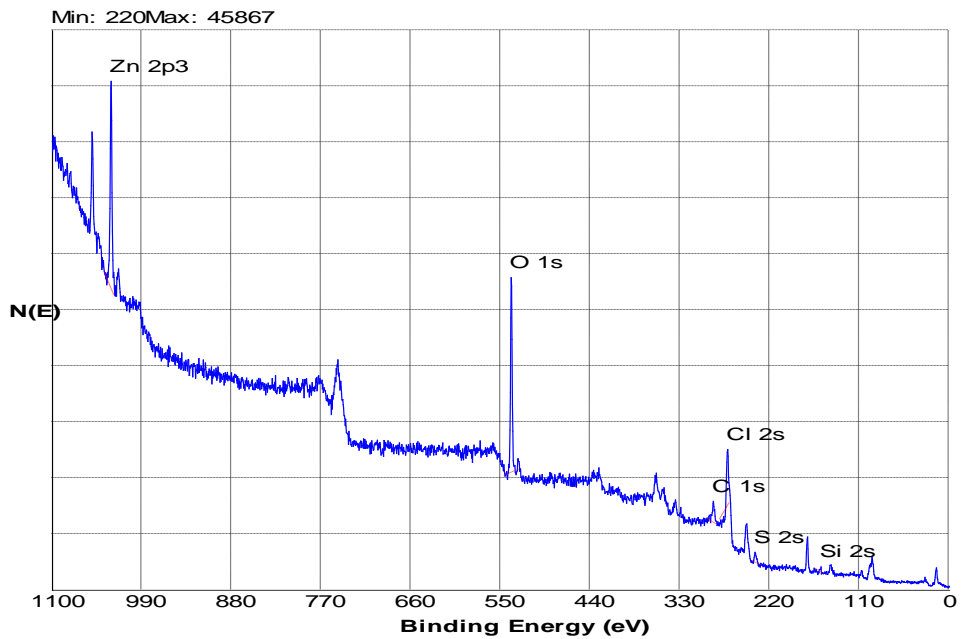


Figure 26: X-ray photoelectron spectroscopy (XPS) survey spectra of C-S ZnSiNP showing the elemental composition.

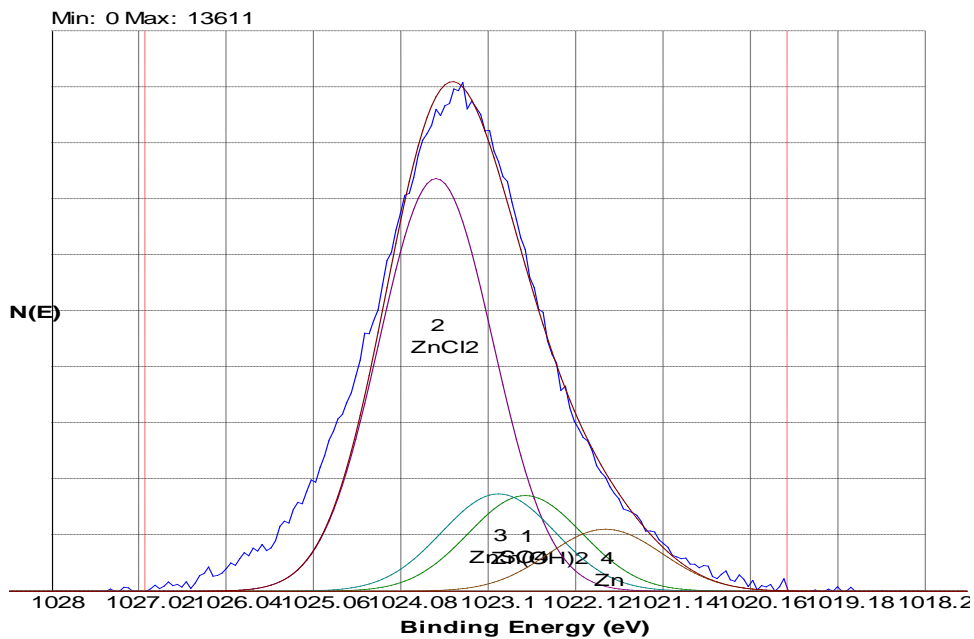


Figure 27: X-ray photoelectron spectroscopy (XPS) high-resolution spectra of Zn in C-S ZnSiNP showing a majority of Zn(II) electron states.

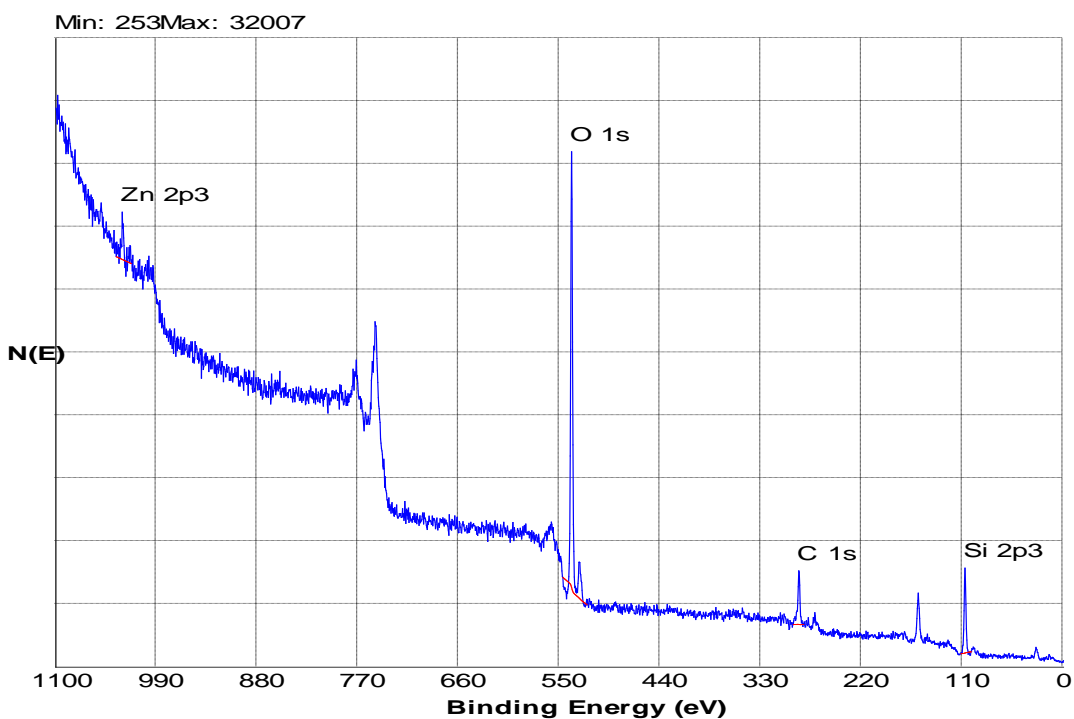


Figure 28: X-ray photoelectron spectroscopy (XPS) survey spectra of ZnSiNG showing the elemental composition.

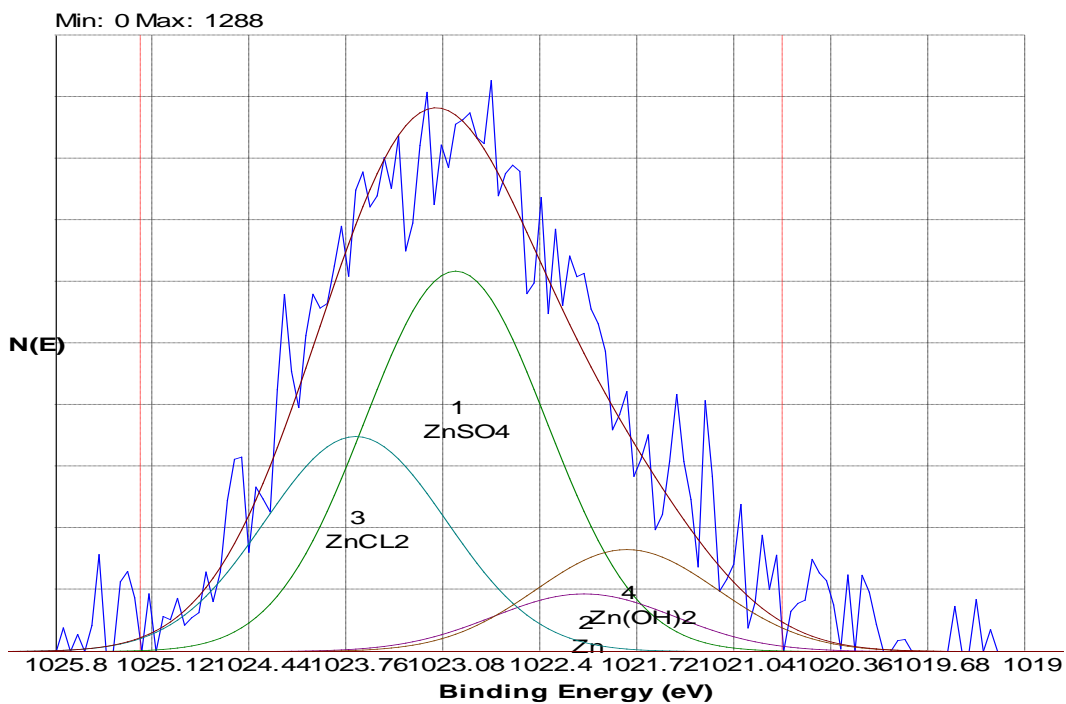


Figure 29: X-ray photoelectron spectroscopy (XPS) high-resolution spectra of Zn in ZnSiNG showing a majority of Zn(II) electron states.



Table 1: Minimum Inhibitory Concentration (MIC) of nanoformulations and controls tested against *X. alfalfae*.

<b>Material</b>	<b>MIC</b>
SiNP	2,500 ppm
C-S SiNP	2,500 ppm
ZnSiNG	39.06 ppm
C-S ZnSiNP*	2,500 ppm
ZnSO <sub>4</sub>	39.06 ppm
Kocide 3000	156.25 ppm
Nordox	78.125 ppm

Table 2: Minimum Inhibitory Concentration (MIC) of nanoformulations and controls tested against *E. coli*

<b>Material</b>	<b>MIC</b>
SiNP	Complete Growth
C-S SiNP	Complete Growth
ZnSiNG	312.5 ppm
C-S ZnSiNP*	10,000 ppm
ZnSO <sub>4</sub>	625 ppm
Kocide 3000	1250 ppm
Nordox	312.5 ppm

Table 3: Minimum Inhibitory Concentration (MIC) of nanoformulations and controls tested against *P. syringae*.

<b>Material</b>	<b>MIC</b>
ZnSiNG	78.125 ppm
ZnSO4	Complete Growth
Kocide 3000	312.5 ppm
Nordox	156.25 ppm

Table 4: Minimum Inhibitory Concentration (MIC) of nanoformulations and controls tested against *C. michiganensis*.

<b>Material</b>	<b>MIC</b>
ZnSiNG	625 ppm
ZnSO <sub>4</sub>	Complete Growth
Kocide 3000	312.5 ppm
Nordox	625 ppm

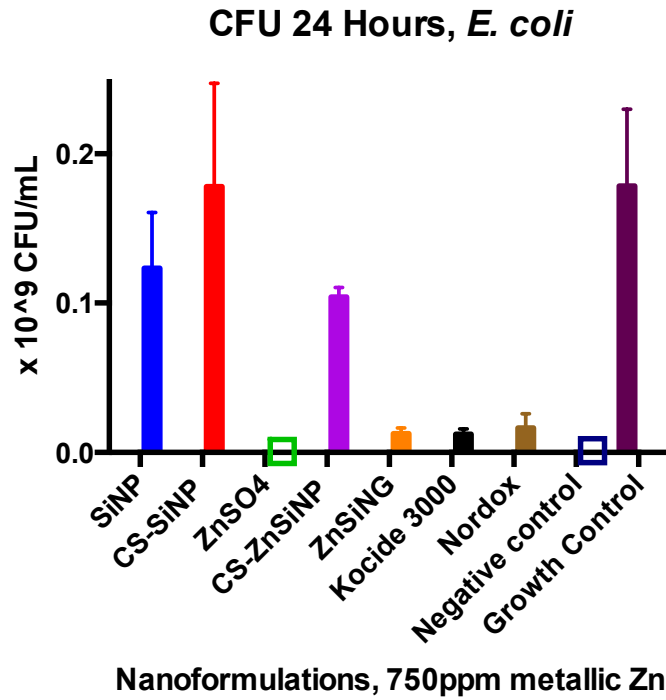


Figure 30: Bar graph of bacterial viability of *E. coli* by SiNP, C-SSiNP, ZnSO<sub>4</sub>, C-SZnSiNP, ZnSiNG, Kocide 3000, and Nordox at 750 ppm of metallic Zn.

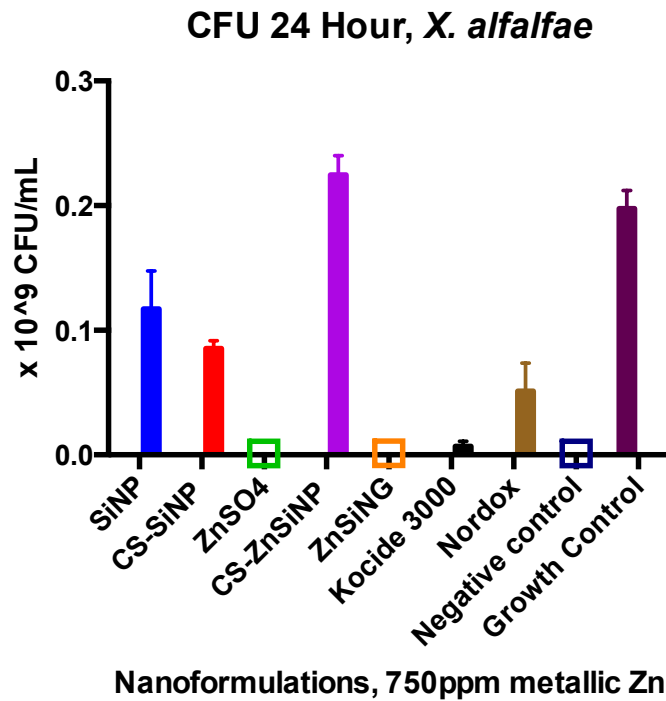


Figure 31: Bar graph of bacterial viability of *X. alfalfae* by SiNP, C-SSiNP, ZnSO<sub>4</sub>, C-SZnSiNP, ZnSiNG, Kocide 3000, and Nordox at 750 ppm of metallic Zn.

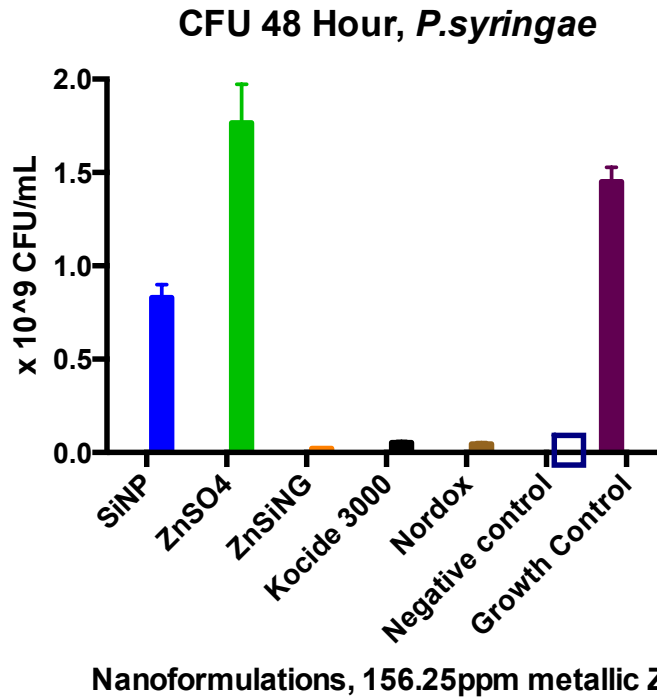


Figure 32: Bar graph of bacterial viability of *P. syringae* by SiNP, C-SSiNP, ZnSO<sub>4</sub>, C-SZnSiNP, ZnSiNG, Kocide 3000, and Nordox at 156.25 ppm of metallic Zn.

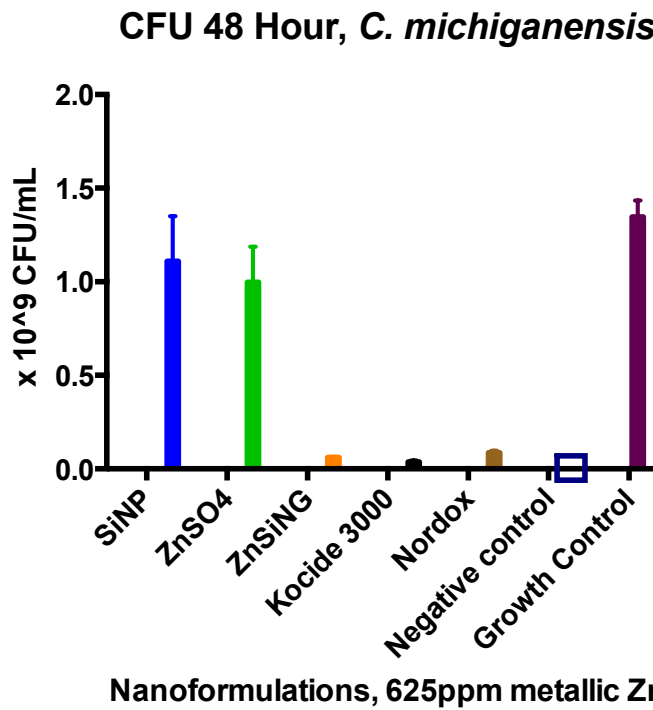


Figure 33: Bar graph of bacterial viability of *C. michiganensis* by SiNP, C-SSiNP, ZnSO<sub>4</sub>, C-SZnSiNP, ZnSiNG, Kocide 3000, and Nordox at 625 ppm of metallic Zn

Table 5: Phytotoxicity rating of nanoformulations against *S. lycopersicum*.

Tested Material	Phytotoxicity Rating		
	24 hr	48 hr	72 hr
Metallic Zn 1000 ppm			
Untreated	-	-	-
SiNP	-	-	-
C-S SiNP	-	-	-
ZnSO <sub>4</sub>	-	-	-
C-S ZnSiNP*	-	-	-
ZnSiNG	-	-	-
Kocide 3000	-	-	-
Nordox	-	-	-
CuSO <sub>4</sub>	+	++	+++

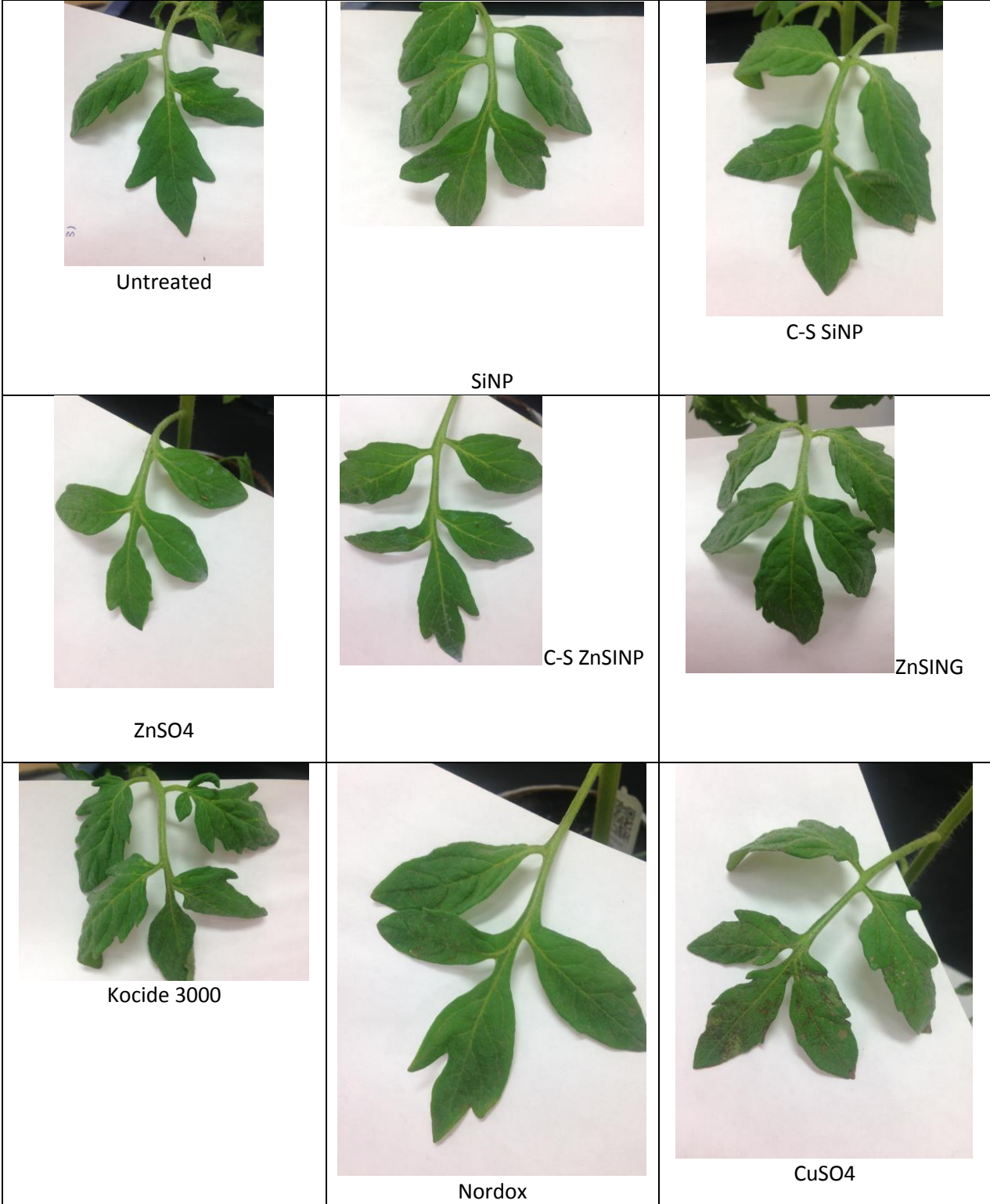


Figure 34: Phytotoxicity testing of nanoformulations against *S. lycopersicum* (photos).



### RAW 24 hours

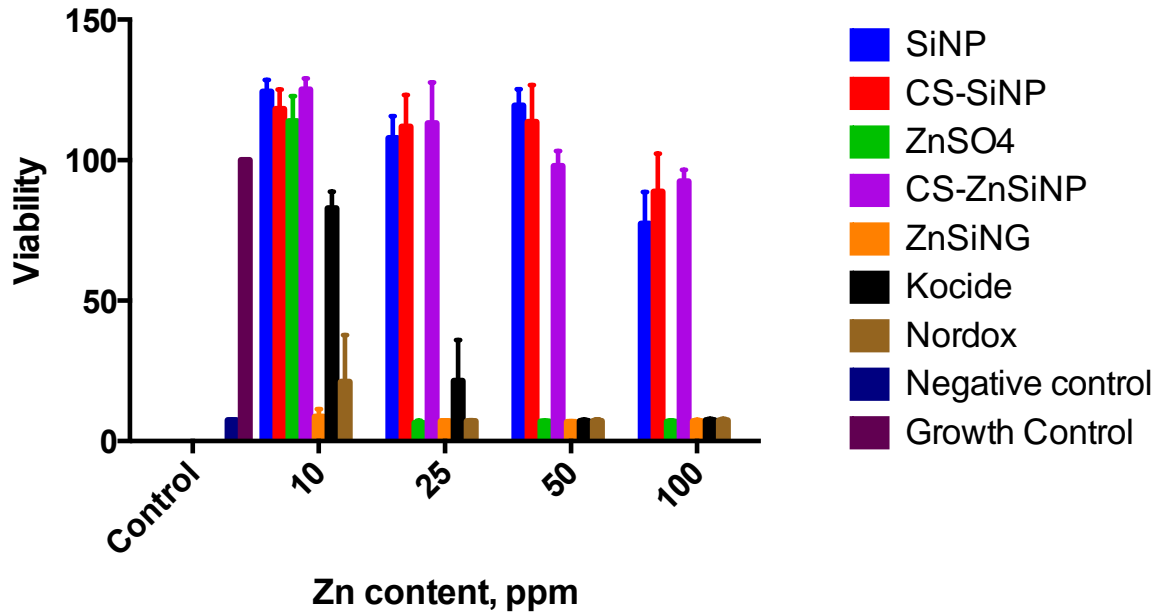


Figure 35: Cytotoxicity data showing comparative effects of ZnSiNG to Kocide 3000 and Nordox on RAW cells.

### A549 Lung Carcinoma Cells 24 hours

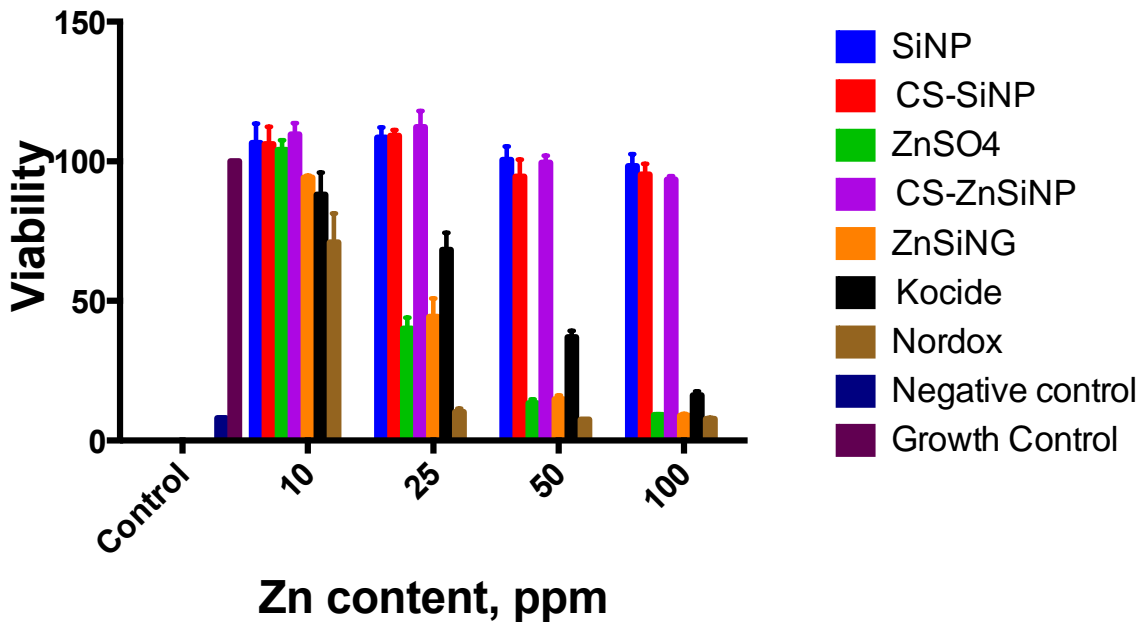


Figure 36: Cytotoxicity data showing comparative effects of ZnSiNG to Kocide 3000 and Nordox on A549 lung carcinoma cells.

## CHAPTER 6: CONCLUSION

The synthesis of C-S ZnSiNP and ZnSiNG was successfully completed following a modified Stober method protocol. SiNP “seeds” were synthesized under basic conditions. Zinc was loaded into the shell via an acidified TEOS solution and ZnSO<sub>4</sub> salt, forming a gel around the core particle. This was completed with and without zinc for comparison. A ZnSiNG was developed as well using a modified protocol from Mikael Young. The nanoparticles solutions were made at high concentration and did precipitate out of solution, but resuspended to form a white, homogeneous solution. Once pH adjusted, the ZnSiNG also forms a white solution.

Characterization of the nanoformulations was carried out using AAS, SEM, HR-TEM, and XPS. AAS data was used to quantify how much metallic zinc was retained after the washing steps in the synthesis of C-S ZnSiNP. Approximately 50% of the zinc was lost after the wash was completed. The metallic zinc concentration of ZnSiNG was calculated by determining the percentage by weight of metallic zinc in ZnSO<sub>4</sub> and final solution. Then the weight is divided by the final volume. The nanogels are not washed therefore no zinc is lost. SEM images showed both the size and shape of the nanoparticles. These were spherical, and approximately 350 nm in size. HR-TEM characterization determined the elemental composition of the particles and gel, while determining the amorphous (non-crystalline) structure of the formulas. XPS data was key in determining the electron states of Zn, which was found to be in primarily the Zn<sup>2+</sup> state with some Zn<sup>0</sup>.

Antimicrobial activity of the various formulas was tested against *X. alfalfae*, *E. coli*, *P. syringae*, and *C. michiganensis*. It became clear that the zinc loading of the C-S ZnSiNP was

not effective enough to develop an effective antimicrobial agent to combat these pathogens. The ZnSiNG, however, demonstrated equally compared to the commercially available products, Kocide 3000 (DuPont) and Nordox (Brandt). One anomaly that was discovered in the testing process was that both *P. syringae* and *C. michiganensis* were able to survive with ZnSO<sub>4</sub> salt at its highest concentration. This may be due to the lower temperature (26 degrees C) of incubation and longer time period (48 hours vs 24 hours) for these experiments. Higher temperature can result in lower pH and higher levels of radical formation, leading to further cellular damage, which was the case with *X. alfalfae* and *E. coli*. MIC and CFU data present similar results in terms of bacterial growth across species.

Current methodologies focus on the use of copper biocides. The overuse of these products has the ability to create drug resistant pathogens and create toxic conditions in the environment. The data compiled in these experiments show potential for the use of zinc-based materials in the agricultural industry to combat disease. *X. alfalfae*, the causative agent in citrus canker, was effectively killed by ZnSiNG. *E. coli* as a hardier test organism, was also killed.

This study also showed promise in the eradication of other important plant pathogens, *P. syringae* and *C. michiganensis*. Phytotoxicity testing reinforced the use of zinc-based materials to combat infection in tomato plants. In a zinc toxicology study performed on *Lycopersicon esculentum* the researchers concluded that at 100 mg kg<sup>-1</sup> level of zinc in the soil is beneficial for growth with 150 mg kg<sup>-1</sup> being toxic (G.Mahalakshmi 2013). Further studies on the beneficial impact of zinc on tomato with the added benefit of pathogen toxicity.

Overall, the ZnSiNG formula performed at a level comparable to the commercial products, with little to variation across species, and no phytotoxicity against tomato plants. This leads to the conclusion that zinc based silica formulas have a future place in the agricultural sector as a replacement for copper.

Further studies on the safety and efficacy of these nanoformulations must be carried out before a decision to mass produce and use in the agricultural field. Cell based plant studies will potentially determine the route of incorporation of these particles based on field spraying and root uptake or incorporation through leaves.

## LIST OF REFERENCES

1. Babich, H. and G. Stotzky (1978). "Toxicity of zinc to fungi, bacteria, and coliphages: influence of chloride ions." Appl Environ Microbiol **36**(6): 906-914.
2. Bader, N. R. (2011). "SAMPLE PREPARATION FOR FLAME ATOMIC  
3. ABSORPTION SPECTROSCOPY: AN OVERVIEW." RASAYAN J. Chem. **4**(1): 7.
4. Bae, C., S. W. Han, Y. R. Song, B. Y. Kim, H. J. Lee, J. M. Lee, I. Yeam, S. Heu and C. S. Oh (2015). "Infection processes of xylem-colonizing pathogenic bacteria: possible explanations for the scarcity of qualitative disease resistance genes against them in crops." Theor Appl Genet **128**(7): 1219-1229.
5. Behlau, F., J. Belasque Jr, J. H. Graham and R. P. Leite Jr (2010). "Effect of frequency of copper applications on control of citrus canker and the yield of young bearing sweet orange trees." Crop Protection **29**(3): 300-305.
6. Behlau, F., B. I. Canteros, G. V. Minsavage, J. B. Jones and J. H. Graham (2011). "Molecular characterization of copper resistance genes from *Xanthomonas citri* subsp. *citri* and *Xanthomonas alfalfae* subsp. *citrumelonis*." Appl Environ Microbiol **77**(12): 4089-4096.
7. Eichenlaub, R. and K. H. Gartemann (2011). "The *Clavibacter michiganensis* subspecies: molecular investigation of gram-positive bacterial plant pathogens." Annu Rev Phytopathol **49**: 445-464.

8. G.Mahalakshmi, P. V. a. (2013). "Zinc Toxicity in Tomato Plants
9. ." World Applied Sciences Journal **24**(5): 649-653.
10. Ghequire, M. G., W. Li, P. Proost, R. Loris and R. De Mot (2012). "Plant lectin-like antibacterial proteins from phytopathogens *Pseudomonas syringae* and *Xanthomonas citri*." Environ Microbiol Rep **4**(4): 373-380.
11. Graham, J. H., T. R. Gottwald, J. Cubero and D. S. Achor (2004). "Xanthomonas axonopodis pv. citri: factors affecting successful eradication of citrus canker." Mol Plant Pathol **5**(1): 1-15.
12. Hsueh, Y. H., W. J. Ke, C. T. Hsieh, K. S. Lin, D. Y. Tzou and C. L. Chiang (2015). "ZnO Nanoparticles Affect *Bacillus subtilis* Cell Growth and Biofilm Formation." PLoS One **10**(6): e0128457.
13. L. Kotz, G. K., P. Tschopel und G. Tolg Z. (1972). Anal. Chem. **260**: 207-209.
14. Maniprasad, P. and S. Santra (2012). "Novel copper (Cu) loaded core-shell silica nanoparticles with improved Cu bioavailability: synthesis, characterization and study of antibacterial properties." J Biomed Nanotechnol **8**(4): 558-566.
15. Mansfield, J., S. Genin, S. Magori, V. Citovsky, M. Sriariyanum, P. Ronald, M. Dow, V. Verdier, S. V. Beer, M. A. Machado, I. Toth, G. Salmond and G. D. Foster (2012). "Top 10 plant pathogenic bacteria in molecular plant pathology." Mol Plant Pathol **13**(6): 614-629.
16. McDevitt, C. A., A. D. Ogunniyi, E. Valkov, M. C. Lawrence, B. Kobe, A. G. McEwan and J. C. Paton (2011). "A molecular mechanism for bacterial susceptibility to zinc." PLoS Pathog **7**(11): e1002357.

17. Moezzi, A., A. M. McDonagh and M. B. Cortie (2012). "Zinc oxide particles: Synthesis, properties and applications." Chemical Engineering Journal **185-186**(0): 1-22.
18. Pelgrift, R. Y. and A. J. Friedman (2013). "Nanotechnology as a therapeutic tool to combat microbial resistance." Adv Drug Deliv Rev **65**(13-14): 1803-1815.
19. Reichman, S. M. (2002). "The Responses of Plants to Metal Toxicity:  
20. A review focusing on Copper, Manganese and Zinc." 22.
21. Rossi, L. M., L. Shi, F. H. Quina and Z. Rosenzweig (2005). "Stober synthesis of monodispersed luminescent silica nanoparticles for bioanalytical assays." Langmuir **21**(10): 4277-4280.
22. Young, M. and S. Santra (2014). "Copper (Cu)-silica nanocomposite containing valence-engineered Cu: a new strategy for improving the antimicrobial efficacy of Cu biocides." J Agric Food Chem **62**(26): 6043-6052.